WIRELESS META-STRUCTURED RF PROBES FOR VIBRATION SENSING

A THESIS SUBMITTED TO

THE GRADUATE SCHOOL OF ENGINEERING AND SCIENCE

OF BILKENT UNIVERSITY

IN PARTIAL FULFILLMENT OF THE REQUIREMENTS FOR

THE DEGREE OF

MASTER OF SCIENCE

IN

ELECTRICAL AND ELECTRONICS ENGINEERING

By

Tuğba Kılıç

July 2023

WIRELESS META-STRUCTURED RF PROBES FOR VIBRATION SENSING
By Tuğba Kılıç
July 2023

We certify that we have read this thesis and that in our opinion it is fully adequate, in scope and in quality, as a thesis for the degree of Master of Science.

Hilmi Volkan Demir(Advisor)

Vakur Behçet Ertürk(Co-Advisor)

Erdinç Tatar

Nihan Kosku Perkgöz

Approved for the Graduate School of Engineering and Science:

Orhan Arıkan
Director of the Graduate School

ABSTRACT

WIRELESS META-STRUCTURED RF PROBES FOR VIBRATION SENSING

Tuğba Kılıç
M.S. in Electrical and Electronics Engineering
Advisor: Hilmi Volkan Demir
Co-Advisor: Vakur Behçet Ertürk
July 2023

Vibration signals are widely used for different monitoring purposes in numerous areas of applications. Sensing vibration and examining its properties play a critically important role essential to damage monitoring especially in the fields of construction and machinery. Detection of possible damages to these structures/machines requires cost-effective and easy-to-use solutions both to protect human health and/or reduce the cost of potential damage to the structures/machines. In this thesis, to offer an efficient and reliable solution for monitoring the health and integrity of various structures and machinery, we proposed and developed a new class of meta-structure based vibration probes that offer high-resolution and real-time wireless monitoring capabilities in vibration sensing. Operating in the radio frequency (RF) domain, this sensor concept relies on the near-field coupling of two nested split ring resonators (NSRRs), each of which is free to move toward each other. In response to the mechanical vibration occurring on a surface to which one of the NSRRs is attached, the amplitude of the electromagnetic wave read out only in vertical direction with respect to the NSRR probe from the coupled-NSRR pair by a transceiver antenna monotonously changes, making the sensing system capable of detecting mechanical vibrations over a wide RF range. The most important advantage of the proposed sensing architecture is that the resonant frequency read-out is very strongly dependent on the spacing between the coupled-NSRR probes, which makes wireless vibration detection at low amplitudes possible. The experimental findings show that this system can wirelessly measure vibration amplitudes as low as 50 μm. Equally important, this opportunely enables a high level of vibration resolution of (differentiation of two close vibration amplitudes separated by) 38.4 μm with an average error rate of only 1.2%. The sensing system exhibits a sensitivity level of 866 kHz/mm. The wireless and passive nature of the proposed system, together with the cost-effectiveness of our NSRR probes, make it highly promising for real-life applications including remote structural health monitoring, deformation detection, and vibration wave monitoring.

Keywords: Wireless passive sensor, vibration sensor, nested split ring resonators, metamaterial-inspired sensor, multi-point sensing.

ÖZET

TİTREİM ALGILAMA İÇİN KABLOSUZ META-YAPILI RF PROBLARI

Tuğba Kılıç
Elektrik ve Elektronik Mühendisliği, Yüksek Lisans
Tez Danışmanı: Hilmi Volkan Demir
Tez Eş-Danışmanı: Vakur Behçet Ertürk
Temmuz 2023

Titreşim sinyalleri, takip etme amaçları için bir çok farklı alanda yaygın olarak kullanılmaktadır. Titreşimi algılamak ve karakteristiğini incelemek, özellikle inşaat ve makine alanlarında hasar bulma ve takibi için kritik öneme sahiptir. Bu yapılara/makinelere gelebilecek olası hasarların tespiti, hem insan sağlığını korumak hem de olası hasarların maliyetini azaltmak için uygun maliyetli ve kullanımı kolay çözümler gerektirir. Bu tezde, çeşitli yapı ve makinelerin sağlığını ve bütünlüğünü izlemek için verimli ve güvenilir bir çözüm sunmak amacıyla, yüksek çözünürlüklü ve gerçek zamanlı kablosuz izleme yetenekleri sunan yeni bir sınıf meta-yapı tabanlı titreşim probları önerdik ve geliştirdik. Radyo frekansı (RF) alanında çalışan bu sensör konsepti, her biri birbirine göre hareket etmekte serbest olan iki tane iç içe bölünmüş halka rezonatörünün (NSRR=Nested Split Ring Resonator) yakın-alan kuplajına dayanır. NSRR'lerden birinin bağlı olduğu bir yüzeyde meydana gelen mekanik titreşime yanıt olarak, bir alıcı-verici anten tarafından NSRR çiftinden okunan elektromanyetik dalganın genliği monoton bir şekilde değişir. Böylece geniş bir RF aralığında sistemin mekanik titreşimleri algılama yeteneğine sahip olmasını sağlar. Düşük genliklerde bile kablosuz titreşim algılamayı mümkün kılan bu algılama mimarisinin en önemli avantajı, eşleşmiş NSRR probları arasındaki boşluğa çok güçlü bir şekilde bağlı olmasıdır. Deneysel bulgular, bu sistemin 50 μm kadar düşük titreşim genliklerini kablosuz olarak ölçebildiğini göstermektedir. Aynı derecede önemli diğer bir durum ise ortalama %1.2'lik hata oranıyla 38.4 μm'lik yüksek düzeyde bir titreşim çözünürlüğü (iki yakın titreşim genliğinin birbirinden ayırt edilebildiği minimum fark) sağlanmasıdır. Bu algılama sistemi, 866 kHz/mm'lik bir hassasiyet seviyesi sunmaktadır. Önerilen sistemin kablosuz ve pasif doğası, NSRR problarımızın maliyet etkinliği ile birlikte, uzaktan yapısal sağlık izleme, deformasyon tespiti

ve titreşim dalgası izleme dahil olmak üzere bir dizi gerçek hayat uygulaması için oldukça umut vericidir.

Anahtar sözcükler: Kablosuz pasif sensör, titreşim sensörü, iç içe bölünmüş halka rezonatörleri, meta malzemeden ilham alan sensör, çok noktalı algılama.

Acknowledgement

I would like to express my sincere gratitude to my advisors Prof. Hilmi Volkan Demir and Prof. Vakur Behçet Ertürk for the continuous support of my study and research, for their patience, motivation, enthusiasm, and immense knowledge. Their scientific eagerness and vision are beyond the words. Their guidance helped me in all the time of research and writing of this thesis.

I would also like to thank Asst. Prof. Erdinç Tatar and Prof. Nihan Kosku Perkgöz for serving on my thesis committee and providing valuable feedback and suggestions. Their insights were instrumental in helping me to shape the discussions of my research work in this thesis.

I would also like to thank TÜBİTAK 121N395 Scholarship Program for the financial support provided during the master's process.

I would also like to thank my colleagues at Demir Research Group for their collaboration during my research. In particular, I would like to thank Emre Ünal, Furkan Şahin and Anıl Çağrı Atak for both their strong support during my thesis work and their sincere and valuable friendship.

I am deeply thankful to family members, my mother, my father and my brothers, for their love and support during this process. Also, I would like to thank to my dear friends who are like sisters. Without their encouragement and motivation, I would not have been able to complete this study.

Finally, I would like to express my deepest and most special thanks to my dear husband, Etka, who has been with me at every moment and in my work for years. His support, understanding and love are my greatest strength. I would not have been able to complete this thesis without him.

Contents

List of Figures

List of Tables

Chapter 1

Introduction

1.1 Motivation and Objectives

Vibration may be generated by a variety of natural and human-made sources. For example, naturally-occurring sources include earthquakes and landslides, while human-induced ones include mining and tunnel excavations. These vibrations can be felt in structures and may cause serious damage. Today vibration measurement has attracted significant attention in the research, design, manufacturing, and maintenance of mechanical structures and products. Differences in the natural vibrations of machinery provide useful information about their mechanical problems. Vibration measurement has also been used as an effective method in designing, manufacturing, monitoring, and maintaining mega-structures such as buildings and bridges. These measurements typically involve measuring various parameters including vibration displacement, velocity and acceleration. A device capable of converting a vibration signal into an electrical signal is commonly referred to as a vibration sensor. Different types of vibration sensors utilizing various physical effects have gained attention, and with advancements in electronics and production processes, a wide range of vibration sensors have emerged for use in diverse fields. These vibration sensors are produced using different methods. However, to the best of our knowledge, there is no account of wireless, passive and easy-to-fabricate vibration sensor providing a micrometer-level resolution, which has been reported to date.

In this thesis, a wireless vibration detection system is proposed and demonstrated. This system may find use in many areas such as determining the operating performance and mechanical damage of machines, structural health monitoring, and fault detection on a surface. Our research team has previously developed the nested split-ring resonator (NSRR), which was specially designed for precise strain measurements with exceptional field localization. This thesis study shows the NSRR architecture for the vibration sensing purposes for the first time. In this thesis, a vibration detection system made of two NSRR probes, paired with a transceiver antenna, operates wirelessly in the RF range. The operating principle of the proposed system is based on the near-field coupling between the antenna and the sensor. This study revealed that the NSRR probes induce a local dip in the reflection response of the antenna at or around its resonant frequency. Furthermore, any mechanical vibration in the sensing probe shifts this dip. This sensor is found to exhibit exceptional sensitivity and resolution, particularly in detecting exceedingly small vibration amplitudes at a micrometer level. Sensitivity decreases when the transceiver moving to the far zone of the NSRR probes. Working in the near zone improves all basic parameters: increasing sensitivity, enhancing resolution, and decreasing error.

1.2 Organization of the Thesis

In the thesis, Chapter 2 reviews the literature and comprehensively discusses metamaterials and vibration sensors. Chapter 3 presents our vibration sensor design with improved NSRR geometry, together with a single-slot microstrip antenna to measure the vibration displacement. In addition, the working principle of the proposed detection system is explained. The placement of the probes and antenna is discussed, and the sensor structure is described. Numerical simulations of the sensor, the antenna and the whole system are provided and their results are explained. In Chapter 4, the experimental characterization of the proposed wireless vibration sensing system is presented. The experimental setup and vibration source are explained. Frequency shifts of the sensor readouts in response to the vibration are shown. In the first stage, the Fourier transform of the results obtained from the sensor is investigated to indicate the accuracy of the sensing system. Also, the vibration characteristics in the time domain can be studied. Various experiments and measurement methods are described to obtain the sensor properties. Using these measurements, the vibration amplitude is calculated in terms of distance between two NSRR probes only in the vertical direction with respect to the NSRR probe. Based on these measurements, the existing figure-of-merits for these vibration sensors including linearity, sensitivity, resolution and errors are presented. Moreover, the distances between the sensor-antenna and between the two NSRR probes are examined. In addition, the range of vibration amplitude that is detected by the sensor structure is investigated depending on the distance between the antenna and the sensor. Chapter 5 presents the concept of a multi-sensor and single-antenna system created with multiple sensors, each with a different resonance frequency. The vibration data obtained from these sensors subject to vibration using different combinations are examined, and comparisons are made. Using a single antenna, many sensors have been seen in the same reflection spectrum. Here it is shown that each sensor can be operated separately without being coupled to the other sensors according to the vibration movement. This thesis concludes with Chapter 6, which summarizes the work and discusses possible improvements as future work.

Chapter 2

Scientific Background

Vibration is a dynamic phenomenon, visually described as an oscillatory motion when the structure is in a balanced position [1-2]. Vibration involves the transfer and storage of mechanical energy, which results from the effects of one or more forces acting on the structure [3]. Vibration measurements typically encompass various parameters such as vibration displacement, velocity, and acceleration. In recent years, vibration measurement has gained significant importance in various aspects of mechanical structural product, design, production, and maintenance. This has resulted in increased attention and focus on vibration sensors, which are designed based on a variety of physical principles [4]. With advancements in various manufacturing technologies, a diversity of vibration sensors have emerged to ensure diverse application areas, leading to continuous development and innovation. There are several types of vibration sensors, but the basic measuring principles involve the detection of vibration parameters through the mechanical structures of objects. These parameters are then converted into electrical signals using physical effects, thereby converting non-electrical signals into electrical signals [5]. Vibration sensors can be classified as displacement (amplitude) sensors, velocity sensors, and acceleration sensors according to the vibration parameters they measure. These three types of sensors are also used interchangeably as displacement, velocity, and acceleration are related by simple calculations.

To detect electrical signals converted from vibrations, inductive sensors can use electromagnetic induction, relying on self-inductance of coils or mutual inductance between the coils. Key features of inductive sensors include their simple and reliable fabrication, high accuracy, excellent stability, and strong output powers. However, they may have limitations in terms of sensitivity, linearity, and range due to mutual constraints making them less suitable for measuring high-frequency dynamic signals [6,7].

Piezoelectric sensors generate their own electricity. They work based on the piezoelectric effect exhibited by certain materials, where vibrations cause the piezoelectric material to generate an electric charge on its surface. This electrical charge is then amplified by a voltage or load amplifier and undergoes impedance transformation into a power output directly proportional to the external force applied to the sensor. This allows the measurement of vibrational parameters. Piezoelectric sensors are mainly used to measure dynamic force and acceleration. With the rapid advancement of electronics technology enabling low noise and high insulation resistance as well as the availability of low capacitance secondary instruments and cables, piezoelectric vibration sensors are increasingly used in a wide range of applications [8].

Another structure for vibration sensing namely magnetic sensors (electrical sensors) are designed to convert vibration parameters into induced electromotive force, thereby converting mechanical energy into electrical energy. These sensors work on the principle of electromagnetic induction. These sensors offer several benefits such as producing significant output signals, requiring straightforward post-processing circuitry, and exhibiting robust anti-interference capabilities. The disadvantages are that they have relatively complex and large structures [9].

A capacitive sensor converts non-electrical vibration signal parameters to capacitance and then converts capacitance to voltage or current using the capacitive effect. Capacitive changes occur depending on the distance between the plates forming the capacitor [3,5]. Capacitive sensors have several remarkable features, including their ability to provide high resolution, wide measuring range, high sensitivity, short dynamic response time, and suitability for online and dynamic measurements, as well as non-contact measurements. [10]. Capacitive sensors also have some disadvantages including a limited measuring range, high output impedance, parasitic capacitance, reduced anti-interference ability, and susceptibility to electrical and electromagnetic fields during measurements. [11]. The capacitive principle can be easily applied to MEMS (micro-electro-mechanical systems) technology. In this application, a charged parallel-plate capacitor that converts mechanical energy into electrical energy is arranged as a spring-mass system. It is important to note that the capacitive principle requires continuous charging of the capacitor to ensure efficient conversion. This can be achieved through a special electronic circuit that charges the capacitor accordingly [12,13].

Another type of sensor is the fiber optic sensor. This type of sensor typically consists of three main components: an optical fiber, a laser, and a light detector. The features of the optical fiber sensor include high sensitivity, fast response, resistance to electromagnetic interference, corrosion resistance, electrical isolation, suitability for long-distance transmission, and seamless integration with computer systems to create telemetry networks using fiber optic transmission. These sensors are particularly suitable for long-range vibration measurements in harsh industrial environments, as they exhibit high sensitivity and reliability in continuous operation, can detect vibration amplitudes as low as 10^{-12} m, and allow three-dimensional vibration measurements. However, a limitation of optical fiber vibration sensors is the narrow measurement frequency range, which offers room for further improvement to expand their capabilities [5,14].

Photoelectric sensors are also examples of vibration sensors. These sensors work by converting weak vibrational parameters to changes in light, which are then converted into electrical signals via optoelectronic devices using the photoelectric effect. This allows the vibration parameters to be converted into power changes [15]. Key features of photoelectric sensors include high resolution, high sensitivity, fast response time, and non-contact operation. In particular, the photoelectric sensors using lasers as light sources and utilizing laser interference and diffraction have been gaining more attention owing to their high sensitivity in optical vibration measurements. However, the limitations of photoelectric sensors include limited measurement distance and the sensitivity of optoelectronic devices to environmental interference, resulting in complex practical applications [16].

Numerous vibration sensor structures utilize the various techniques discussed above, finding applications in various areas of daily life. One notable application is the continuous recording of ground movements for determining the critical parameters of the ground movement such as magnitude, duration, center, and time of ground shaking, which are typically achieved using seismometers to detect earthquake-induced ground vibrations. The principle of seismic accelerometers is based on the measurement of vibratory acceleration [17]. While seismic sensing technology is well-established, alternative methods for detecting ground vibrations are not commonly found in the literature. Recently, sensing-focused structures inspired by metamaterials have shown potential in various sensing applications such as biosensing, strain sensing, pressure detection, temperature sensing, and structural health monitoring [18-23,27]. Attempts have also been made to manipulate the resonant frequency, particularly in the terahertz range, by altering the structural elements of the resonator or external physical parameters [23-26]. MEMS technology, especially utilizing piezoelectric and capacitive sensing techniques, has gained prominence in vibration sensors and finds applications in diverse fields [28].

Metamaterials (MMs) are artificial (or human-made) structures with carefully selected elements whose dimensions are comparable to or smaller than the wavelength (λ) of the incident electromagnetic wave. The change in the electromagnetic response of the incident wave depends on two fundamental parameters of these carefully selected elements: permittivity (ϵ) and permeability (μ) of their material, which is unique for each chosen material based on its atomic configuration. Metamaterials, regardless of the component materials, give a unique electromagnetic response and thus behave like new materials. Therefore, in metamaterials, each structure exhibits dipole properties similar to atoms in natural materials, causing either ϵ or μ or both to be negative. Also, almost all natural materials have positive ϵ and μ across the electromagnetic spectrum, with the exception of metals (negative ϵ close to visible frequencies) and ferrites (negative μ at low frequencies) [36]. Veselago introduced the concept of left-handed materials

(LHMs), which are materials that have both negative permittivity and negative permeability in 1968. In LHMs, the propagation directions of phase velocity and group velocity are opposite. Split-ring resonators (SRRs) were proposed by Pendry et al. to achieve negative permeability in 1996 [29]. SRRs, which may serve as the basic components of LHMs, have been extensively studied in the literature and different SRR designs are presented such as complementary split ring resonators (CSRR) [37], closed ring resonators (CRR) [38], broadside coupled split resonators (BCSRR) [31], multi-split ring resonator (MSRR) [21], and comb-like split ring resonators [21, 31]. SRRs have found applications in sensing, serving as biosensors [30], strain and displacement sensors, as well as thin-film sensors [31]. The sensing mechanism of a metamaterial sensor relies on the change of transmission/reflection coefficients with respect to frequency/wavelength or quality-factor (Q factor). Our group previously reported a new nested geometry of the SRRs, which our group coined NSRR [31]. The NSRR structure is particularly effective for achieving precise strain measurements owing to its exceptional sensitivity and field localization.

Apart from these purposes, the vibration-sensing structure was designed with the BCSRR structure reported in [33] and [34]. In [33], the given structure is based on perceiving the vibration caused by walking, running, or falling from a height of a heavy object by placing the BCSRR structure mutually. Another study investigates the potential of utilizing to detect mechanical vibrations [34]. Here the SRR structure acts as a vibration sensor, where the amplitude of the interacting electromagnetic wave in the GHz frequency range is directly modified based on the amplitude of the mechanical vibration using the BCSRR. The BCSRR unit, integrated into the microwave transmission system, is capable of vibrating its rings in response to mechanical vibrations. A comprehensive qualitative formulation of the process was presented along with experimental validation of different degradation possibilities. The proposed use of the BCSRR as a sensitive vibration sensor holds great potential for real-life applications.

Considering the aforementioned vibration sensors and, in particular, metamaterial-based sensors, in this thesis, a new class of wireless sensing system that can detect mechanical vibration using NSRR has been shown for the first time. The NSRR structure used in the vibration detection system here was previously proposed and developed by our group [21,31]. The strong dependency of the resonance frequency on the spacing between the two coupled NSRRs in response to the vibration amplitude is the main idea behind the operating principle of our proposed system makes it an ideal candidate among different SRR structures for wireless vibration sensing [34, 35].

Chapter 3

Wireless Sensing System Modeling and Design

3.1 Design of Sensing System Components

3.1.1 Nested Split Ring Resonator Design

The design of a NSRR that looks like two combs was first reported by Melik et al. for the purpose of obtaining higher sensitivity and a smaller footprint compared to typical SRRs [31], and it is used in this thesis study as the heart of the sensing structure. New designs were obtained by changing the number of strips, dielectric substrate used, and fabrication method on the structure given in [31], which is the starting point of our design. The frequency range called ultra high frequency (UHF), which includes many applications in the RF range, was used as the frequency operating region because UHF is considered quite reasonable in structural health monitoring applications [43], which is one of the recommended usage fields for our sensing architecture. In addition, the application of structural health monitoring has the highest reflection coefficient at various frequencies, and one of them is 400 MHz [43]. Therefore, the 300-500 MHz range was used within this band. Our proposed sensing system can be used in various applications by changing the sensor dimensions and obtaining the desired frequency. An initial design working at the desired resonance frequency was determined [42], where the equivalent circuit model of the NSRR structure is presented in great detail. Final design is then achieved using full wave solvers.

The NSRR comprises numerous parallel strip pairs that are interconnected on one side but symmetrically separated on the other side by a gap between each pair. Each strip forms a pathway with the uppermost strip that is split by the gap. Consequently, the entire structure can be considered as a combination of nested split rings. By increasing the number of strips, the NSRR can be made electrically smaller, which enhances the overall capacitance and inductance of the structure and lowers its resonance frequency. Additionally, a high-Q resonator characteristic can be achieved by increasing the number of gaps, thereby resulting in enhanced sensitivity and resolution. In a prior investigation conducted by our research group, the NSRR design for wireless measurement of strain in biological sensing research allows for the monitoring of the structure's strain as it is conveyed to the sensor [20]. However, this necessitated the sensor to undergo stretching or contracting, limiting the detection capability based on Young's modulus of the sensor material. The NSRR substrate is primarily composed of a dielectric material. In a separate group study, a structure was employed by modifying the NSRR probe to detect the tension and stress exerted on the rebars [21]. This investigation allowed for obtaining information regarding the elastic and plastic deformation [40]. Within this investigation, the NSRR probe was partitioned into two parts over the gaps between the strips, and the two sections were connected using a wire. As a result of this design, the wire serves as a constraining element.

In this work, the metamaterial architecture of the sensing probe is composed of a NSRR. Each configuration is designed with the goal of achieving high sensitivity and high resolution. The sensor structure is created using two NSRR probes. These two NSRR probes are placed face to face with each other. Thus, a sensor could be obtained. A fabricated NSRR probe is shown in Figure 3.1 and the sensor structure and dimension are given in Figure 3.2(a) and 3.2(b), respectively. There are copper strips on the NSRR probe and a gap between each strip. While these strips create an inductive effect, gaps create a capacitive effect. It has fixed capacitive and inductive values due to the probe design. The capacitive effect could be observed from the distance change between the two plates of the sensor. One of the NSRR probes is attached to the structure whose vibration is measured, and the other plate is fixed.

In the design part, various substrate materials were used, and it was seen that the best option for sensitivity and resolution is Rogers materials. During the preliminary measurements, Rogers RO4730G3 gave the best results in terms of durability during the adhesion to the surface. The number of strips on the NSRR was determined according to the desired resonance frequencies. In the general system, the number of strips on the probe was determined by considering the antenna operating range, antenna-probe size relationship, and the most appropriate frequency values in the environment to be used. When two NSRR probes are placed face to face, the distance between the two plates is set to d.

Four sensors having different resonance frequencies were designed. The strip numbers and footprints of these sensors are all different. Therefore, their resonance frequencies are expectedly distinct. The dielectric thickness of the substrate used for our design should not be thicker than 0.55 mm and its relative dielectric constant (ε_r) should be 3 or less because the sensors produced using these features ensure that there is no inter-coupling between the sensors within the multi-point sensing architecture (see Chapter 5), and exhibit the best operating performance. To meet these requirements, the NSRR probes were built on a single-sided Rogers RO4730G3 substrate with $\varepsilon_r = 3$ and a thickness of 0.53 mm. The dimensions of the NSRR probe can be seen in Figure 3.2(b): The width (W) of the probe was 52.00 mm while its length (L) was 47.20 mm. On the probe, the width of each copper lines (L_{mp}) was fixed at 0.80 mm, and the length of each finger (W_{mp}) was set to be 23.83 mm. The distance between the strips (L_a) was 0.8 mm and (W_a) 1.14 mm. Also, the distance between the outermost strips and the edges of the substrate (W_b) was 0.80 mm. The strip at the top (W_m), which was not divided into two, is 50.40 mm. The details of the used sensors can be seen in Table 2.1. The probes were designed with the use of the licensed program CST Microwave Studio, and probes with the desired resonance frequency were obtained by changing the physical dimensions. Sensing probes were etched onto a single-sided Rogers RO4730G3 substrate by using LPKF ProtoMat Circuit Board Plotter after the design was obtained.

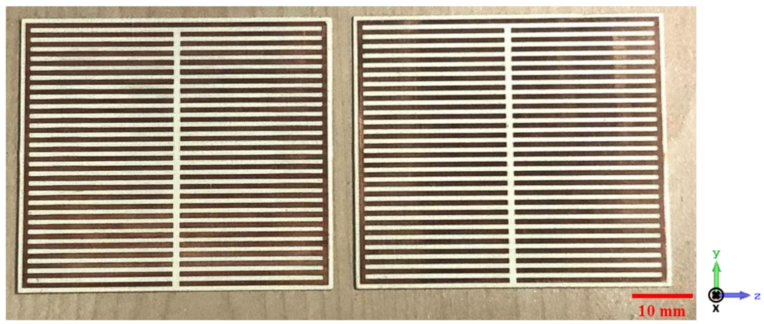

Figure 3.1: Our fabricated NSRR probes. Two identical NSRR probes are used to make one sensor.

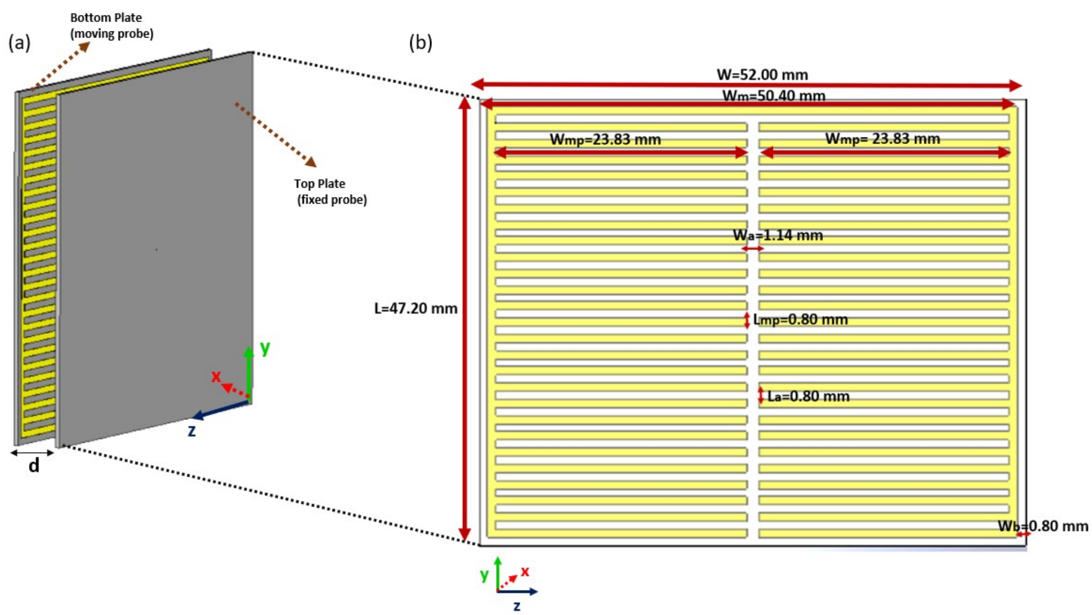

Figure 3.2: (a) Sensor structure, the upper and lower plates are positioned opposite each other. (b) Geometry of NSRR probe.

Table 3.1: Information on four sensors named according to the number of strips and their different areas due to the varying number of strips. Different resonance frequencies due to the varying metal number and gap amount.

Number of Sensor Strips	Footprint	Resonance Frequency
25	42.4 x 52.0 mm	461.6 MHz
26	44.0 x 52.0 mm	453.6 MHz
27	45.0 x 52.0 mm	429.8 MHz
28	47.2 x 52.0 mm	423.8 MHz

3.1.2 Antenna Part

In the measurement, an interrogating single-slot microstrip antenna re-designed according to the specifications given in the reference [41] is used. The configuration depicted in Figure 3.3 employs a modified single-slot microstrip antenna operating at a frequency of 445 MHz with a bandwidth of roughly 5 % and $|S_{11}| < -10$ dB.

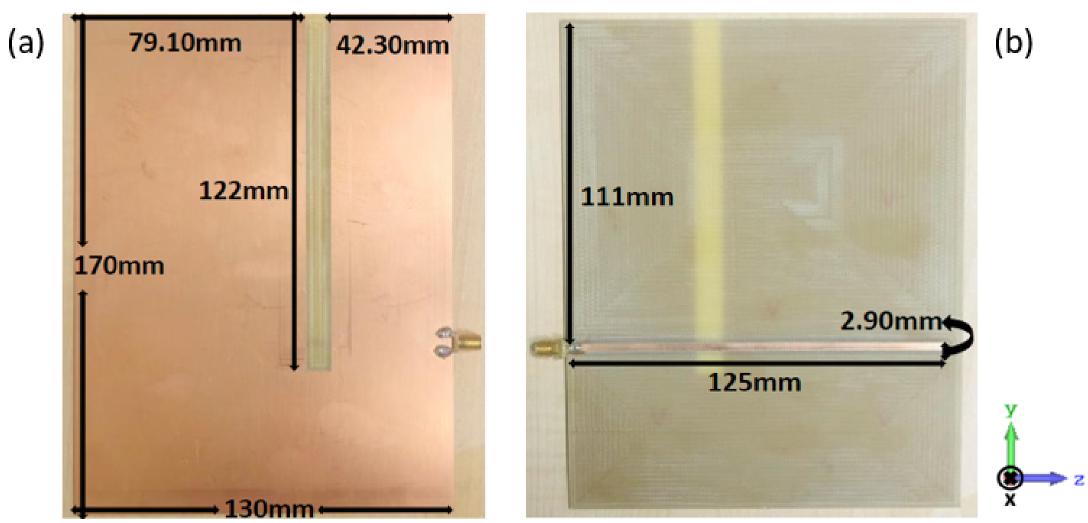

Figure 3.3: Microstrip single-slot antenna design parameters: a) the slot part in the front side (b) the feed-line in the backside.

The selection of this particular antenna type is primarily attributed to its ability to offer a significantly reduced size relative to the wavelength, as well as an expanded bandwidth. The 50 Ω microstrip feed line for the microstrip slot antenna is situated at one end of the dielectric substrate. On the opposite side, there is a ground plane with a monopole slot. By inserting a slot on the opposite side of the substrate, an E-field polarized in the z-direction is created between the slot and the NSRRs probes, which are also z-directed. Consequently, the antenna and NSRRs are highly coupled. Using an NSRR reduces the probe size considerably compared to the working wavelength. This is advantageous since a smaller, more compact probe can be used on thinner and smaller structural components. Figure 3.3 shows the design parameters of the microstrip single-slot antenna, while Figure 3.4 depicts the reflection coefficient (S_{11}) of both its measurement and simulation results.

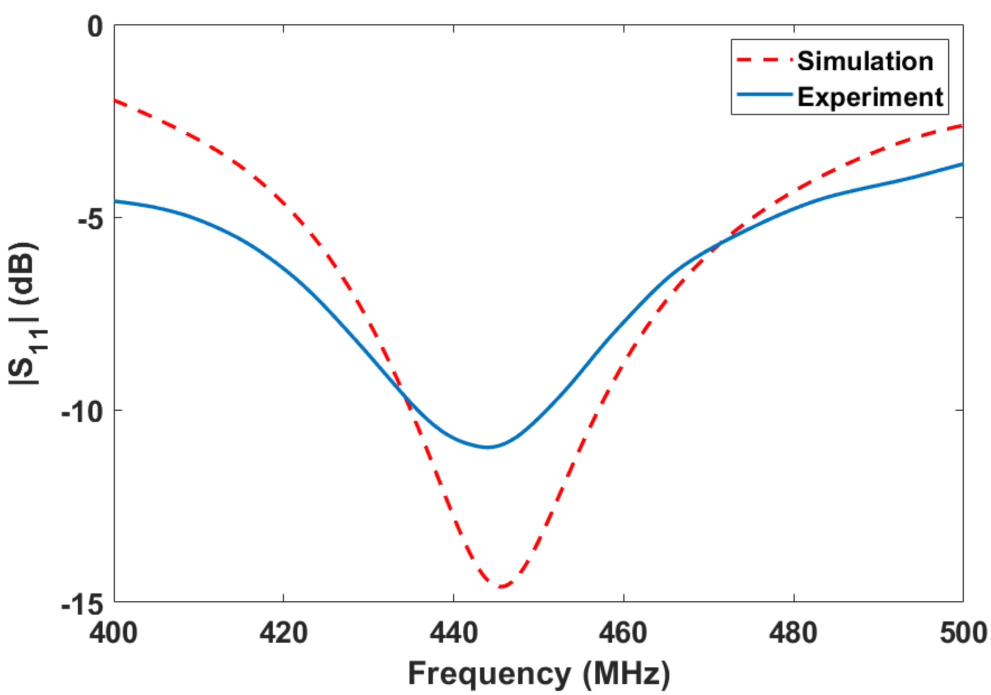

Figure 3.4: Measured and simulated reflection coefficient vs. frequency for the microstrip single-slot antenna.

3.2 Operation Principles of the Sensing System

The sensing system operates on the principle of electromagnetic coupling of the NSRR probes with the antenna. Any alterations to the NSRR probes are immediately reflected in the antenna's reflection coefficient, resulting from this coupling.

At its resonance frequency, the NSRR probe specifically produces a distinctive feature on the antenna's reflection characteristics in the form of a local peak or dip. Mechanical variations of the NSRR probes, such as the displacement between the two sensor plates, can be traced in the peak or dip.

In the installed system, the principle of wireless vibration detection is based on tracking capacitive changes. When a vibration comes to the ground or surface, the probe affixed to this surface starts to move with the vibration. Movement occurs on the surface as much as the amplitude of the incoming vibration. Therefore, the sensor part (NSRR probe attached to the ground) moves by this vibration amplitude amount. This movement causes the distance d between the two plates of the sensor to change. This distance change causes the capacitance change of the capacitor, in a very similar to parallel plate capacitor formula $C = \epsilon A/d$, where $\varepsilon_{\mathrm{r}}\varepsilon_0$ because type is air between the two NSRR probes. When d changes, the capacitance changes. Capacitance change causes frequency change by $f = 1/(2\pi\sqrt{LC})$ formula. In the antenna reflection spectrum, a change in frequency values is observed as a peak or dip point where we see the presence of the sensor. Also, the sensor resonance frequency used must be within or near the antenna operating band. When the sensor resonance frequency is within the antenna working band, the system sensitivity value increases considerably. However, the sensor can still be sensed even if it is not in the band but close to it.

The antenna that serves as the sensing system's transceiver has the sensor probe in its near-field. It transmits the waves to the sensor and gathers the backscattered signal from the network analyzer. The excitation technique used is what causes the significant coupling between the NSRR probe and the antenna that was seen. This excitation mode facilitates a well-coupled system, where the splits and gaps are aligned horizontally with the antenna. The resultant strong electromagnetic coupling leads to enhanced sensitivity and resolution.

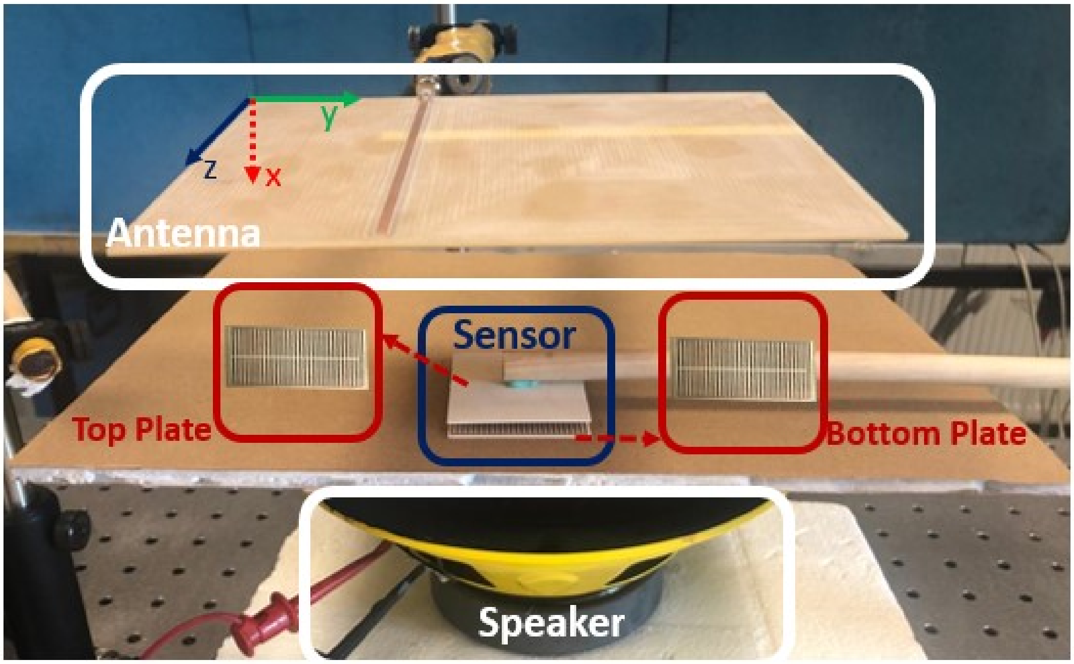

Figure 3.5: The image of the antenna and sensor in the experimental setup. The sensor consists of two identical plates. The plates are set face to face. One plate is glued to the surface, and the other is fixed with the help of rods. An antenna at a certain distance from the sensor receives the data.

3.3 Numerical Simulation

Numerical investigations were systematically carried out by utilizing the transient solver of the commercial CAD software CST Microwave Studio to forecast this behavior and understand how it functions. Initially, the process of designing and simulating sensors was executed. The sensors designed at the desired frequencies and dimensions were simulated in a waveguide under appropriate excitation and boundary conditions. As depicted in Figure 3.6, the sensors were positioned at the center of the waveguide. As long as the waveguide dimensions are larger than the sensor dimension, it gives smooth results. The sensor must be subject to the most suitable excitation and boundary conditions within the waveguide. Boundary conditions are selected as follows: the strips of the sensor must be parallel to the electric field lines. These field lines run along the strips and the spaces between the strips. Magnetic field lines are chosen to be perpendicular to these fields. A suitably excited sensor provides maximum coupling with the fields thanks to these configurations. The selected boundary conditions for this scenario specified that the lateral surfaces, with normal vector components of +/- z direction were taken as perfect magnetic conductors (PMCs), which set the tangential component of the magnetic field to zero. The top (+y direction) and bottom (-y direction) surfaces are selected as perfect electric conductors (PECs), which set the tangential component of the electric field to zero. This choice of boundary conditions results in a plane wave propagation where the magnetic and electrical fields are both perpendicular to the direction of propagation (in the x direction) and perpendicular to each other. You can see the waveguide simulation setup in Figure 3.6.

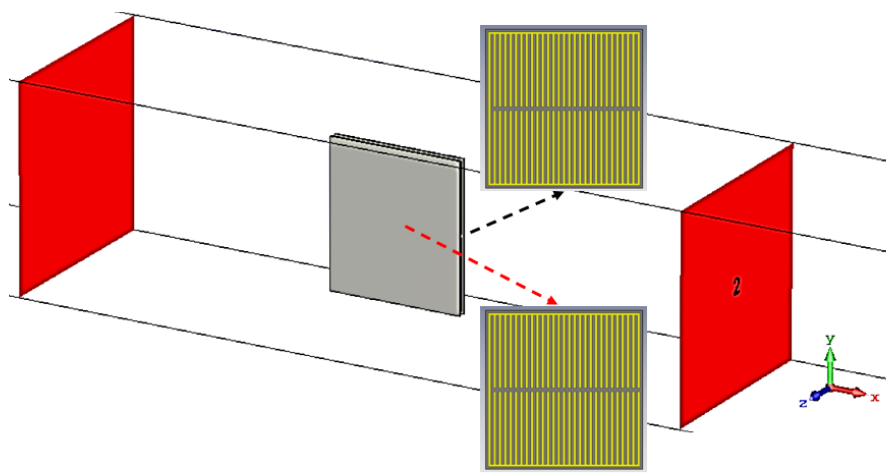

Figure 3.6: Waveguide simulation setup to determine the resonance frequency of the sensor.

Using the aforementioned configuration, simulations were conducted for each sensor, and the resonance frequencies of each sensor were determined and tabulated in Table 3.1. Figure 3.7(a) illustrates the simulation result of 28-strip sensors within the waveguide. It is necessary for the resonance frequencies of each sensor should be in or near the antenna operating band. Figure 3.7(b) indicates that both the antenna and sensors operate within the same frequency band. Antenna operating frequency range is generally considered to be the frequency range that includes magnitudes of -10 dB and below. It is known that sensors whose resonance frequency is in the antenna operating frequency range are suitable for working with this antenna. The findings of this study indicate that the sensor can operate beyond its designated operating band. However, a loss of antenna-sensor coupling strength occurs.

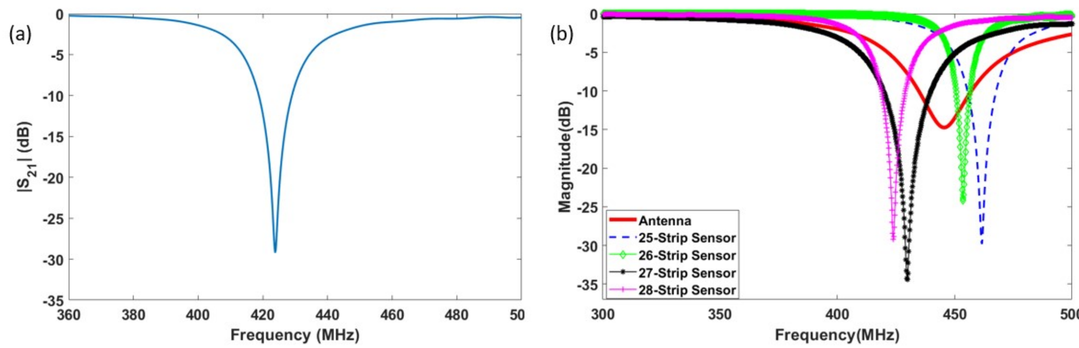

Figure 3.7: (a) Waveguide simulation for 28-strip sensor. (b) Antenna reflection vs. sensor resonance frequency. Sensor frequencies are within the antenna operating range.

Within the waveguide, the distance between the two plates was manually modified to reflect changes in the vibration amplitude. One of the plates was held stationary while the other was moved, thereby adjusting the distance d between them and allowing for the observation of corresponding frequency changes. As predicted, decreasing the distance between the two plates increases the capacitance value and causes a subsequent shift in frequency towards lower values (Figure 3.8).

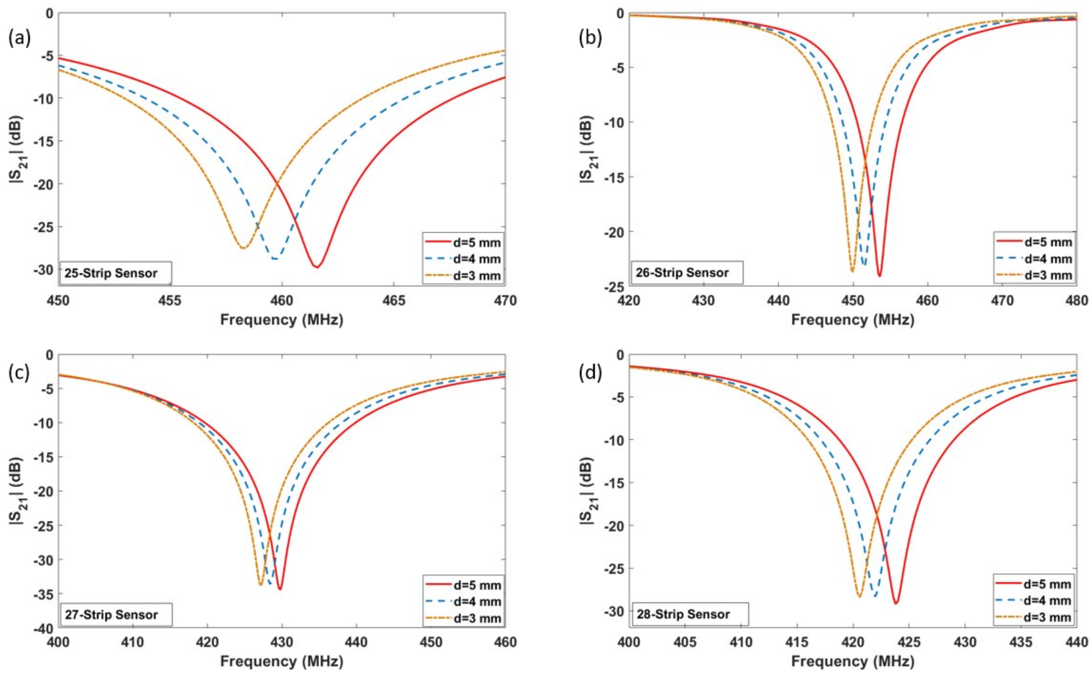

Figure 3.8: Waveguide simulations of frequency shifting for (a) 25-strip sensor, (b) 26-strip sensor, (c) 27-strip sensor, and (d) 28-strip sensor.

The sensing system is primarily composed of two fundamental components: the antenna and the vibration sensor. The operational functionality of the system is influenced by several factors such as the positioning of the antenna and sensor, the distance between the antenna and sensor, and the maximum range of the distance between the sensor probes. The sensor is positioned across from the antenna slot to ensure the best possible interaction between the antenna and sensor. As mentioned before in the waveguide simulation, the electric field component of the antenna and the strips on the sensor are parallel to each other and the best coupling is provided between the system elements. The distance between the antenna and the sensor, known as the monitoring distance (D_m), which will be mentioned later, is a crucial parameter that significantly affects the sensing system. To determine the optimal positions for the antenna and sensor, simulations were conducted by placing the sensors at varying distances. The simulation studies were carried out to compare the characterization of the electric fields on the NSRR probes in the antenna's near-field region. The monitoring distance was set to 8 cm, as seen in Figure 3.9(a), and the electric field localization is shown in Figure 3.9(b), where the magnitudes of electric fields are quite substantial. Although these values do not entirely reflect the actual values, they serve as valuable references for comparison purposes. Another critical parameter that influences the sensing system is the distance between the sensor parts, denoted as d. A reference value of 5 mm was established for d value, and for all sensors, the distance d was set between 5-6 mm in both simulations and experiments since while the system has maximum linearity in the range of 1-7 mm, the linearity of the system decreases as d increases.

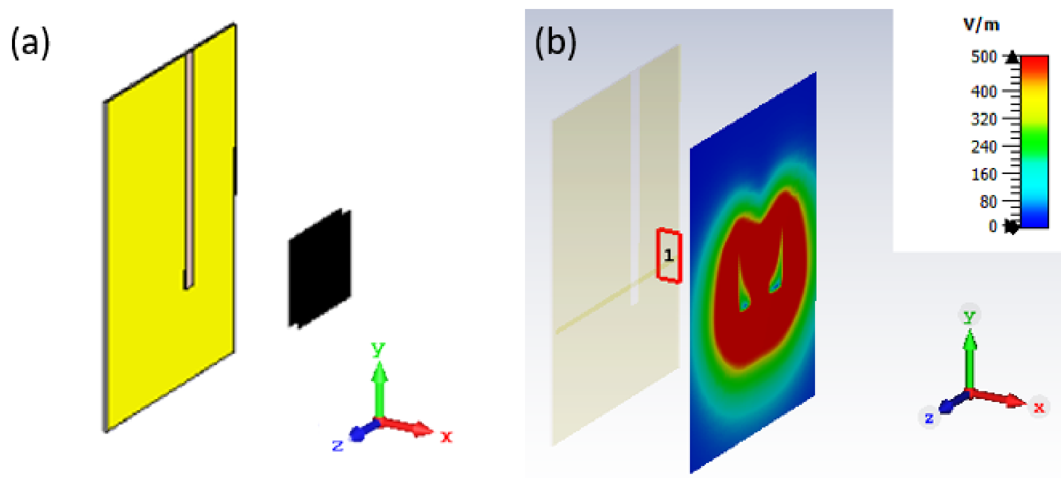

Figure 3.9: (a) Antenna sensor location and (b) numerically calculated electric field when the distance between the sensor plates is 5 mm and the distance between the system elements (antenna and sensor) is 8 cm.

A separate sensing system was installed with each sensor and antenna. The antenna sensor system's response showed itself as a dip or a peak in the antenna's reflection spectrum. Since each sensor has a different resonance frequency and is seen as a dip or a peak around this resonance frequency in the antenna-sensor system, the systems can be easily distinguished. As observed in Figures 3.10(a) and (b), by trying to imitate the change in the distance between the two plates depending on the vibration amplitude, frequency shifts were observed as the dip or peak in the reflection coefficient of the antenna. In Figure 3.10, frequency shifts occurring at the sensor response points are observed depending on the distance between the probes.

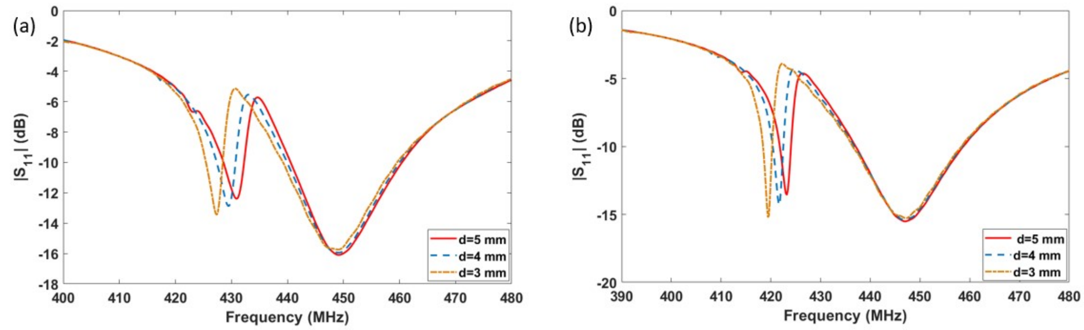

Figure 3.10: Frequency shift in response to the variation in the distance d between two plates for (a) 27-strip and (b) 28-strip sensor.

Chapter 4

Characterization of the Sensing System with a Single Nested Split Ring Resonator Pair

Before implementing the sensing system in a practical environment, it is imperative to make a comprehensive characterization of its electromagnetic behaviour. Various experimental methodologies were used to gain insight into the properties of the system using a single NSRR pair. An experimental setup was built to detect the vibration. There are several ways to generate vibration. A speaker source was chosen as the vibration source in order to induce the vibration acting on the sensor in a controlled way. The speaker was fed with a signal generator. In this way, the desired signal type could be applied to the speaker easily. Moreover, different amplitude and different frequency values could be applied. In fact, using two signal generators at the same time, signals of different amplitudes and frequencies could be used. Many different combinations could be created in terms of the applied amplitude, frequency, and signal types. Thus, vibration signals that are more complex than the simple ones can be generated and used in the system in a controlled way.

The signal is transmitted to the coil part of the speaker, which is connected to the signal generator. At the top of the speaker, there is a circular diaphragm with a cylindrical core in the middle and a voice coil wound on top of it. The electric current on this coil causes vibration in the diaphragm. The cone part is the moving part. A leg made of plastic, which is a very light material, was placed on the cone. On this leg, a flat cardboard surface whose dielectric constant is very close to the dielectric constant of air was placed. Thus, the vibration movement in the speaker according to the incoming signal is transmitted to this flat surface. One NSRR probe of the sensor was attached to this flat cardboard surface. The other sensor part was fixed with a wooden stick, and the distance d between these two parts was set to 5-6 mm. The antenna was placed at a distance of 8 cm from the fixed sensor as shown in Figure 3.5. As mentioned in the simulations section, the antenna and the sensor were positioned in the same way. Thus, the best interaction between the two main elements was achieved. To collect data from the antenna, we used a network analyzer (Agilent FieldFox N9915A) as the signal acquisition instrument and tuned it to the operating frequency range of the antenna. Data extraction speed is critical for our experiments since we need to detect the vibration in transient. It is necessary to capture the transient changes with the network analyzer we use. IF bandwidth (IFBW) and the number of data points are critical parameters that affect the speed of measurements. Decreasing IFBW reduces the effect of noise. The higher the IFBW, the greater the noise. Each tenfold reduction in IFBW width lowers the noise floor by 10 dB. However, a narrower IFBW results in longer sweep times. Therefore, the data extraction speed slows down. The IFBW is set to 100 kHz so that the maximum sweep time is 43 ms. Error time in the data extraction is defined that the difference between the time that should take to retrieve each data and the time that can be retrieved from the network analyzer due to speed. The network analyzer is triggered every 1.001 seconds, which is most optimal time for applied vibration frequency range 0 to 1 kHz, but the data may not be fully received during this time. Data acquisition time is recorded via MATLAB and error time is found by taking difference between 1.001 seconds and data acquisition time. It is 3.25-37 μs, which is quite acceptable for this experiment. Another important parameter, number of data points, was determined to increase the speed. The higher the data points, the higher the resolution, but taking too many data points slows down the measurements considerably. Therefore, it is set to 101 data points to record data quickly without losing too much information. Changing the number of data points does not affect the error time. With these adjustments, we could observe the vibration with a sweep time of approximately 90 ms. The experimental setup is presented in Figure 4.1.

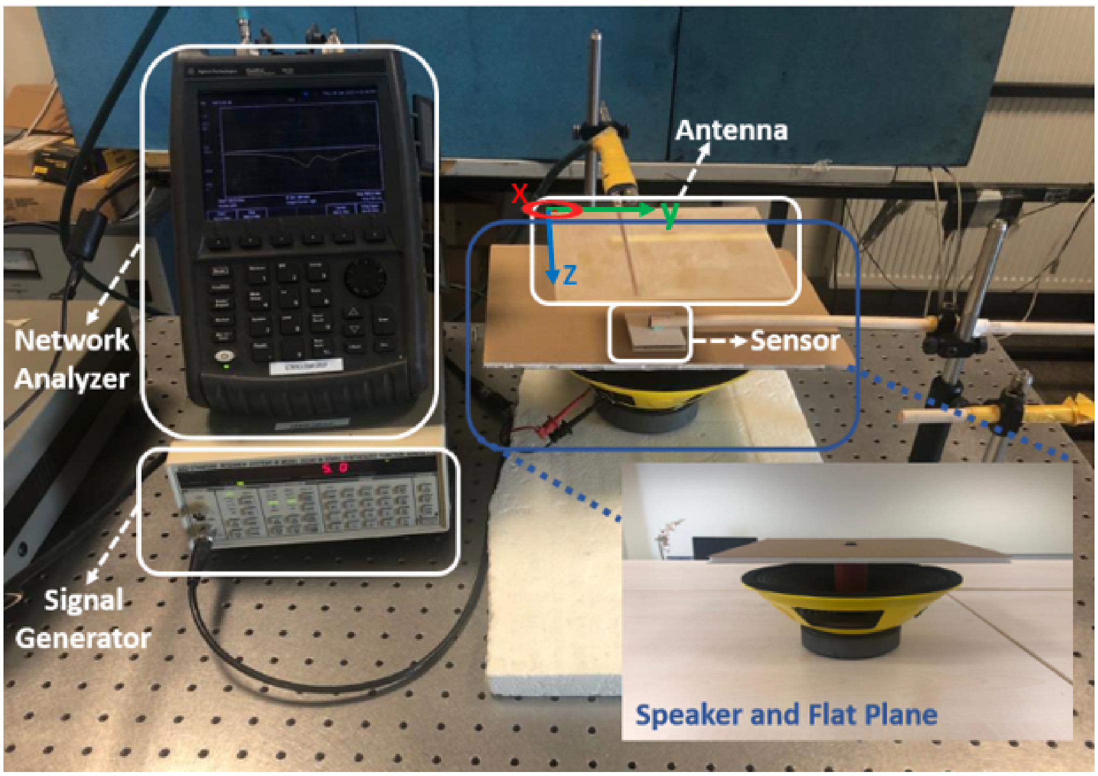

Figure 4.1: Our experimental setup. The vibration sensor was placed on the speaker, a pick-up transceiver antenna was used to read out the sensor signal. The network analyzer was set to scan in the frequency range from 300 to 500 MHz recording 101 data points. Signals of different types, amplitudes, and frequencies were applied to the mechanical system and the RF data was recorded using the network analyzer.

In the system, sensors at different resonance frequencies were recorded in the antenna reflection spectrum as seen in Figure 4.2. Each sensor exhibits a dip around its resonance frequency value so that differences in different sensors and systems can be easily seen. Different types of signals can be applied using the signal generator. A sinusoidal signal was chosen as the most ideal signal type for performance evaluations. When it is applied to the speaker, the amplitude change of the signal causes up and down motion on the sensor. The amplitude change of the applied signal corresponds to the vibration amplitude. The frequency value of the signal determines the speed of this movement. This movement due to amplitude change activates the sensor attached to the surface and changes the distance d between it and the fixed part. This distance change causes a capacitive change in the system and is observed as a frequency shift by dip in the S_{11} response of the antenna and the frequency of this dip shifts as the vibration amplitude changes, as can be seen in the frequency shift in Figure 4.3. As the vibration amplitude (signal amplitude) increases, the amount of frequency shift increases. Depending on the incoming vibration amplitude, the maximum and minimum frequency values are determined in the frequency shift. The difference between these two values is the frequency shift (Δf). By using Δf, the sensor's figure-of-merit and error calculations can be carried out.

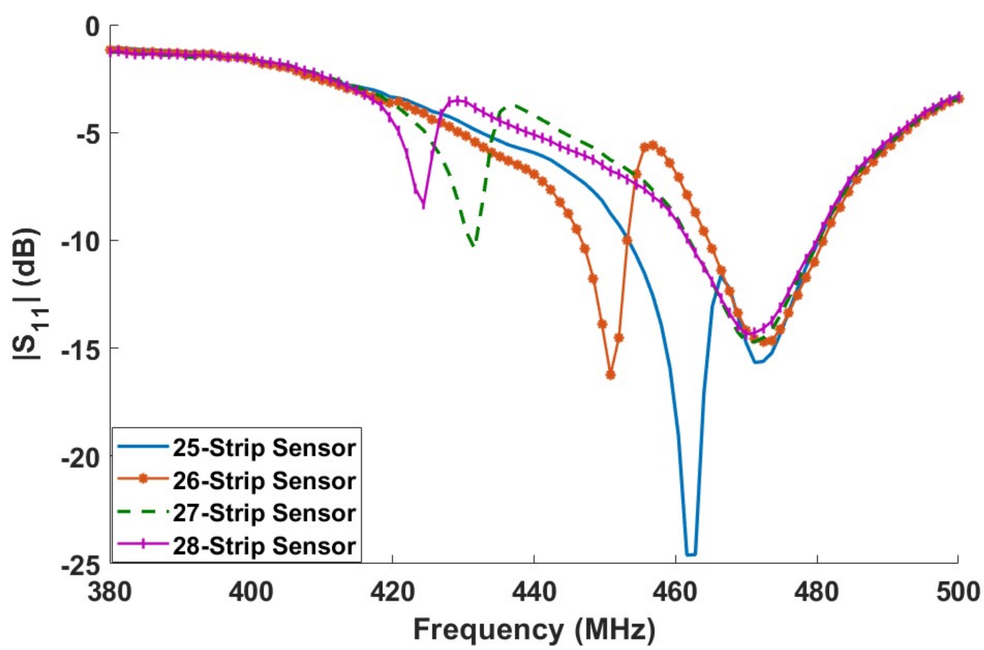

Figure 4.2: Reflection spectrum of the systems installed separately using each sensor. Each sensor gives as a peak or a dip around its own resonance frequency.

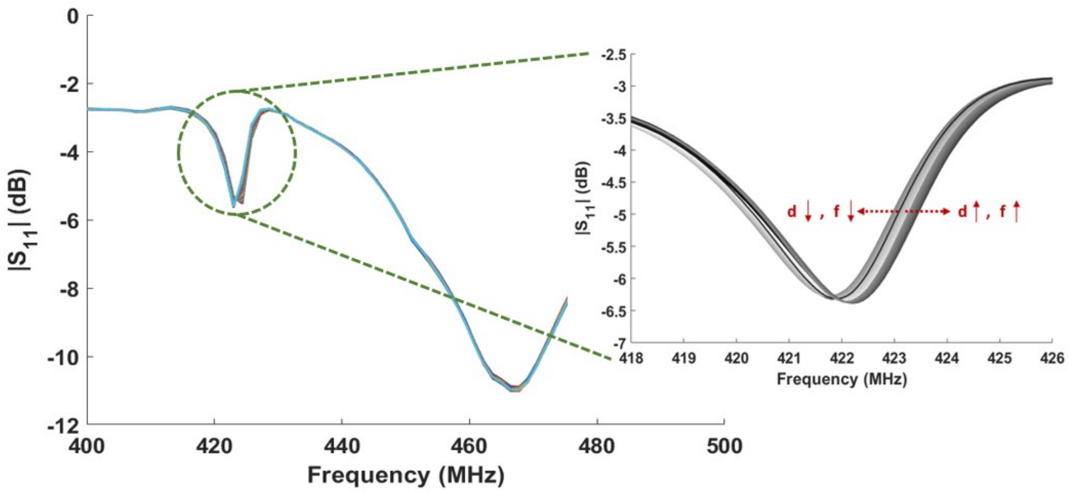

Figure 4.3: Vibration causing frequency shift in the reflection spectrum for 28-strip sensor.

While the movement of the sensor depending on the incoming amplitude of the vibration causes frequency shift in the frequency domain, the applied sinusoidal signal is easily visible in the output in the time domain. The experiment was carried out in such a way that frequency shifts can be seen in the frequency domain. However, the signal was also recorded in time. For instance, a sinusoidal vibration signal with frequency of 5 Hz and amplitude of 10 V_{pp} is applied to the system for 300 s. During this time, both frequency shifts can be seen in the frequency domain and the response can be recorded in time domain. This sinusoidal signal applied to the sensor as the input from the signal generator, is easily visible at the output via the VNA using the antenna. By conducting the time domain analysis, we acquired information about the vibration characteristics. Various types of vibration signals, including triangular, sinusoidal, and rectangular, could be applied. These signals could have different amplitudes and frequencies. Different amplitude and frequency values could also be easily analyzed in time domain, as seen in Figure 4.4(a) and 4.4(b). Fourier transform (FT) was taken to numerically examine the detected vibration. In this way, the amplitude and frequency of the vibrations affecting the sensor could be obtained. To illustrate this process, two sinusoidal vibration signals were separately applied to the sensor, each with a different amplitude but at the same frequency. Subsequently, FT was performed, leading to the visualization of the vibration characteristics shown in

Figure 4.4(c). It was observed that vibrations with varying amplitude values but the same frequency exhibited the maximum amplitudes at the applied frequency value. Additionally, the results from both the time domain and FT analysis verified the proper functioning of the system.

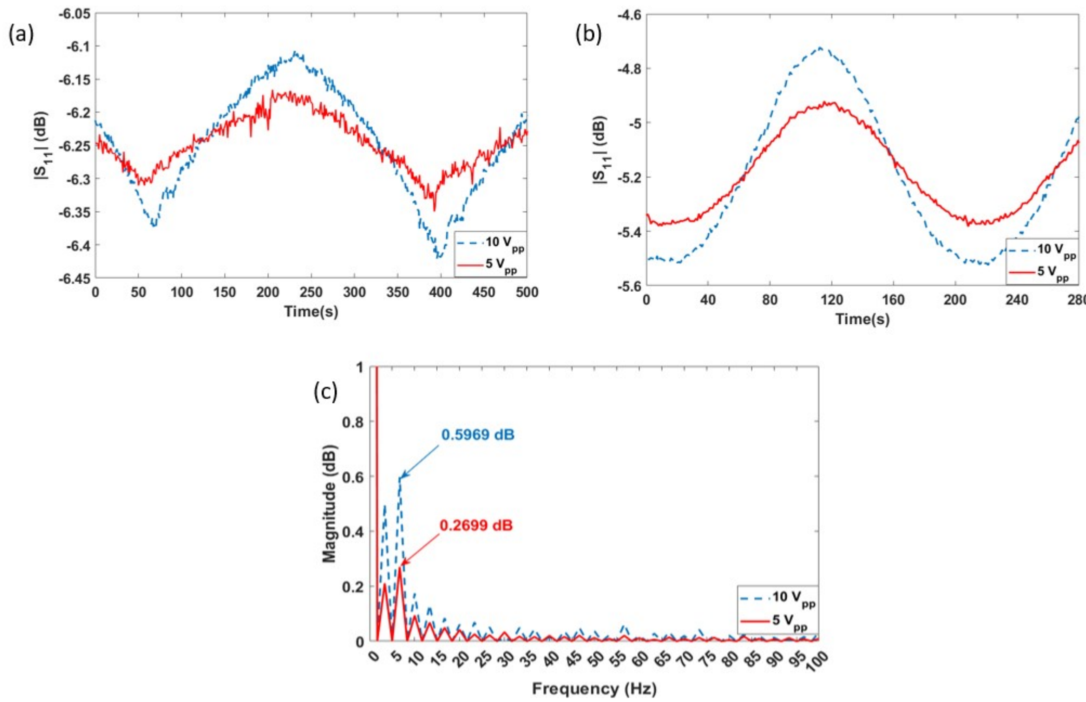

Figure 4.4: (a) Time domain measurements for two triangular waves of 5 Hz−10 V_{pp} and 5 Hz−5 V_{pp}, and (b) for two sinusoidal waves of 5 Hz−10 V_{pp} and 5 Hz−5 V_{pp} applied to the sensor (c) Fourier transform analysis of time domain measurements using 5 Hz−10 V_{pp} and 5 Hz−5 V_{pp} sinusoidal vibration signals.

4.1 Linearity and Coupling NSRR Probe of Pair

Linearity between the amplitude of vibration (operating voltage applied by the signal generator) and frequency value of dip can be assessed through a statistical metric known as the coefficient of determination, or R^2. The definition of R^2 is given in Appendix A. R^2, which ranges from 0 to 1, indicates good linearity when its value is close to 1. The vibration amplitude applied to the sensor with the signal generator was varied between 1-10 V_{pp} and the frequency shift was noted for each case. As the vibration amplitude was increased, the frequency shift was expected to increase as well. This trend was observed in our experiments, shown in Figure 4.5. It was obtained that, as the input increased (decreased) in the system, the output accordingly increased (decreased) and the change was linear. This was achieved at a very high linearity value. R^2 values are given for 4 different sensors in Table 4.1.

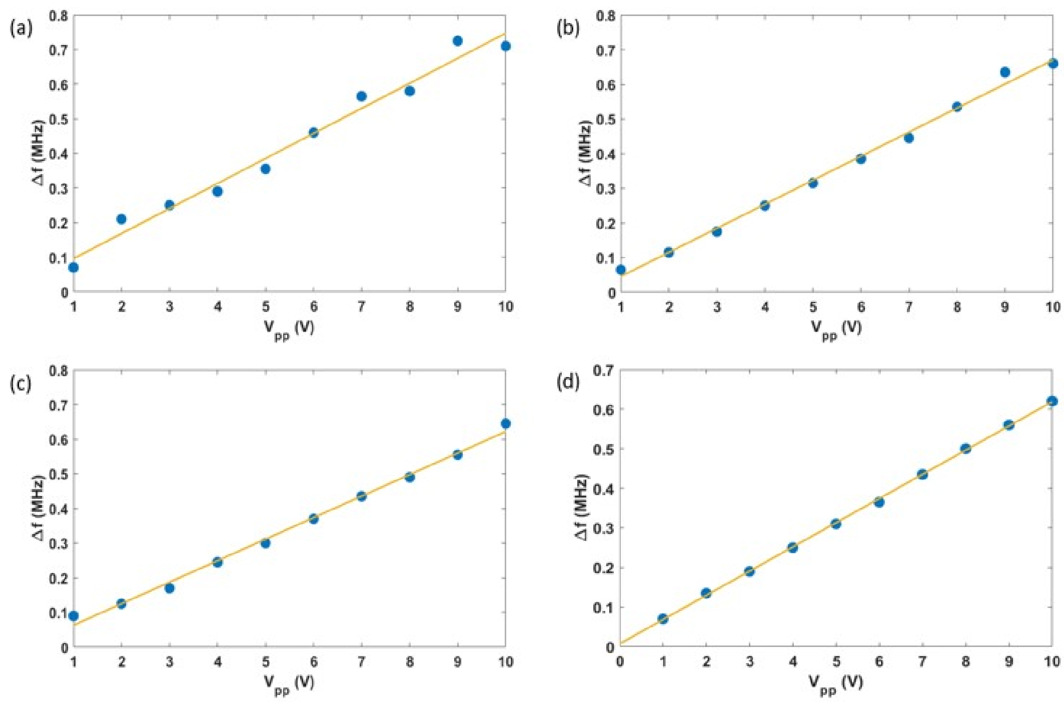

Figure 4.5: Variation of frequency shift measured as a function of the applied voltage for (a) 25- (b) 26- (c) 27-, and (d) 28-strip sensor.

Table 4.1: Degree of linearity exhibited by various sensors for the voltage-frequency shift (Δf) curves presented in Figure 4.5.

Range (V_{pp})	Sensors	R^2
1-10	25-strip Sensor	0.978
1-10	26-strip Sensor	0.994
1-10	27-strip Sensor	0.994
1-10	28-strip Sensor	0.999

Another point to consider in order to use the system with high linearity is the distance d between the two probes. The vibration sensor is designed by positioning two NSRR probes facing each other. As mentioned before, the distance d between these two probes is an important parameter in capacitance value of the sensor. As Figure 4.6(a) illustrates, as the distance between the probes increases, the dip to be tracked shifts to higher frequencies. However, after $d = 9$ mm, we observed two dips in the spectrum. When the frequency shift of these two dips examined, both provide the same and expected results. Nevertheless, we decided to follow the same dip for each d value. As d increases, frequency value of the dip point is expected to increase, while after $d = 30$ mm the frequency value remains constant, as seen in Figure 4.6(b). This value gives the maximum value for d, from which the 0-30 mm range for d is defined as the range where the response is linear. However, as the d value increases, the linearity of the system decreases in various ranges. Table 4.2 tabulates the R^2 values at different d intervals, which provides information about the level of linearity. This parameter quantifies the degree to which an actual curve deviates from a fitted linear curve. The 1-7 mm range has a fairly high R^2 value, and experiments were performed at this $d = 5-6$ mm condition. The value where d is the maximum also defines the maximum vibration amplitude that can be detected by the system. To ensure that vibration is detected effectively, the distance between the plates must be within a range that includes the minimum and maximum amplitudes of the incident vibration. For example, if the maximum amplitude of vibration is 3 mm, the distance between the probes should be at least 3 mm or more.

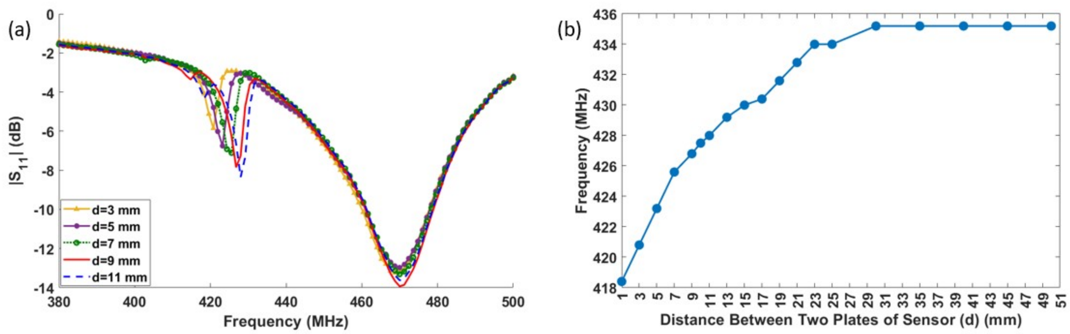

Figure 4.6: (a) Change in the frequency dip in response to the change in distance between two coupled NSRR probes. (b) Frequency read-out varied as a function of d distance (for 28-strip sensor).

Table 4.2: Linearity for various d distances.

d (mm)	R^2
1-7	0.999
9-13	0.997
15-21	0.960
23-30	0.923
1-30	0.889

4.2 Imaging Vibration Amplitude

The vibration amplitude is controlled by the applied voltage obtained from the signal generator in the experimental setup. We need to know the relation between this voltage value (its amplitude) and the actual distance between the NSRR probes. Thus, we performed an independent experiment to obtain this distance information so that we can assess some other performance metrics of our sensor. For this purpose, we used the Nikon D5200 DSLR camera with 24MP (6000×4000 pixels) and 2MP (1920×1080 pixels) resolutions for photo and video modes, respectively. The camera focuses on the probes from the side to measure the distance between the minimum and maximum points at each different voltage amplitude when different voltages are applied. The system is slowed down to capture motion and extract the distance information. Therefore, the speed of vibration has been slowed down 0.1 Hz, and the amplitude value proportional to the voltage applied by the signal generator was obtained in terms of the distance. This experiment was repeated for each voltage value. The corresponding distance information is shown in Figure 4.7(b).

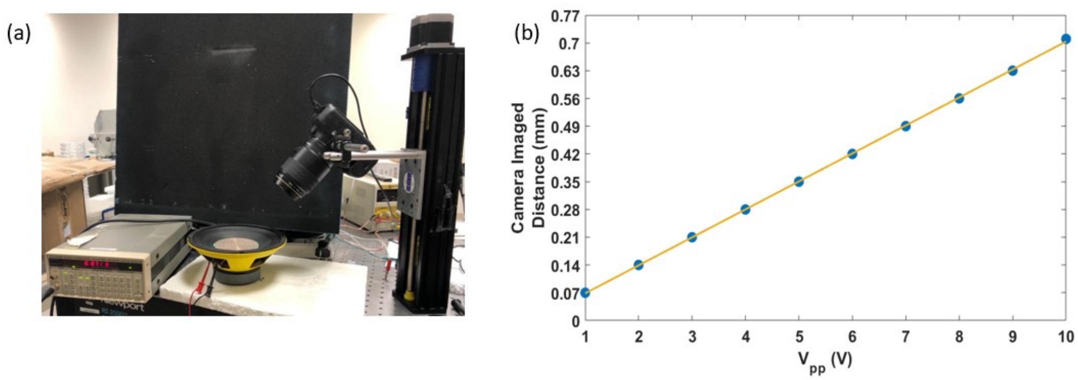

Figure 4.7: (a) Experimental setup used to find the distance as a function of the applied voltage. The amplitude between the speaker's maximum and minimum movement points is measured. (b) Distance vs the applied voltage.

Upon obtaining the distance information as a function of the applied to voltage, it is crucial to access the distance information as a function of measured frequency shifts at each voltage value. In other words, how much distance variation leads to how much frequency shift can be expressed and formulated. To achieve this goal, the slopes of the linearity graphs of Δf vs the applied voltage and the distance vs the applied voltage are used. As an example, Figures 4.8(a) to 4.8(c) illustrate two procedures for the 28-strip sensors.

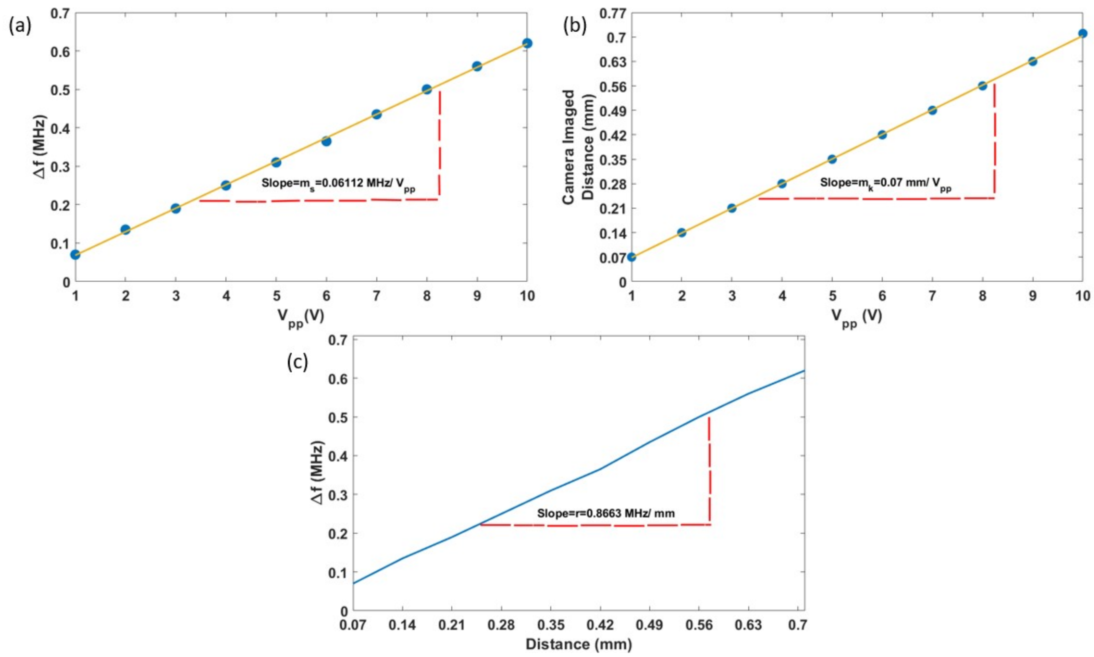

Figure 4.8: (a) Measured frequency shift vs the applied voltage for 28-strip sensors and (b) imaged distance the applied voltage and (c) measured frequency shift vs imaged distance obtained by combining (a) and (b).

The relation of the slope of Figure 4.8(c), to those of Figure 4.8(a) and 4.8(b), m_s and m_k, are given in (4.1). This slope information specific to the NSRR probes and wireless sensing system setting, r, is then used to convert the measured frequency shift to the correspondence distance variation, $d$ist, as given in (4.2).

$$r = \frac{m_s}{m_k}(\frac{MHz}{mm}) \tag{4.1}$$

$$dist = \frac{\Delta f}{r}(mm) \tag{4.2}$$

When the *dist* is calculated using this frequency shift, it is expected to obtain the applied vibration amplitude information within margins of error. In Figure 4.9, frequency shifts depending on the applied voltage value of each system were created using four different sensors, and the distance information based on this frequency shift is displayed for each case. The voltage values applied and the distance values obtained for different sensors are given in Table 4.3. This table shows the operating performance of the wireless system comparing the actual and measured the distances.

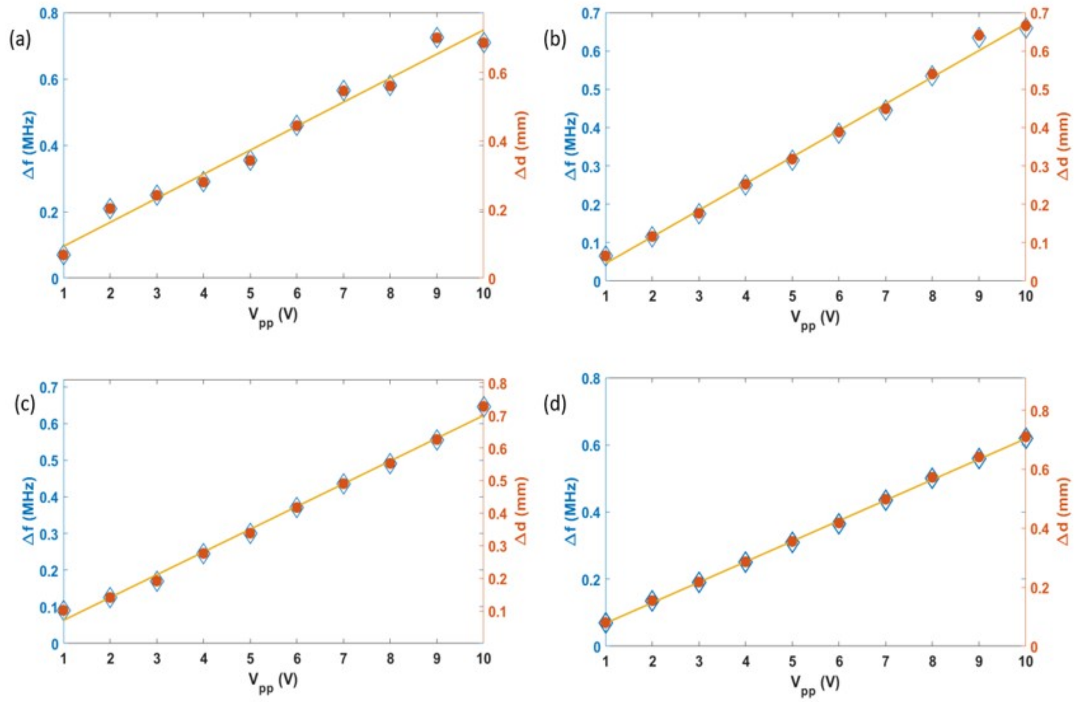

Figure 4.9: Measuring frequency shift for each applied voltage using (a) 25-, (b) 26-, (c) 27- and (d) 28-strip sensors, respectively.

Table 4.3: Comparison of vibration amplitude values and expected values in units of (mm) obtained with each sensor.

V_{pp} (V)	Actual Distance (mm)	Measured Distance for 25-strip Sensor (mm)	Measured Distance for 26-strip Sensor (mm)	Measured Distance for 27-strip Sensor (mm)	Measured Distance for 28-strip Sensor (mm)
10	0.71	0.686	0.665	0.727	0.710
9	0.63	0.701	0.640	0.625	0.641
8	0.56	0.561	0.539	0.552	0.572
7	0.49	0.546	0.448	0.490	0.498
6	0.42	0.445	0.388	0.417	0.418
5	0.35	0.343	0.317	0.388	0.355
4	0.28	0.280	0.252	0.276	0.286
3	0.21	0.241	0.176	0.191	0.217
2	0.14	0.203	0.116	0.140	0.154
1	0.07	0.067	0.065	0.101	0.080

4.3 Monitoring Distance and Vibration Amplitude Tracking Range

The monitoring distance (D_m) refers to the distance between the NSRR probes and the transceiver antenna. Within the monitoring distance of the sensing system, NSRR probes should be strongly coupled to the antenna so that the amplitude change of the vibration can be wirelessly tracked. The antenna-to-probes distance has a significant impact on the sensing system. As illustrated in Figure 4.10, as the monitoring distance increases, the sensor's visibility in the reflection spectrum begins to vanish, and after a certain point, the dip or peak caused by the sensor disappears. The graph indicates that when D_m is 8 cm, the sensor can be effectively sensed. The magnitude value at the frequency dip starts to decrease when D_m is changed from 8 cm to 16 cm. Until this value (D_m=16 cm), different vibration amplitude can be sensed as a frequency shift throughout the entire range (in the experimental range). After 16 cm, the dip point caused by the sensor vanishes, and the frequency shift attributable to vibration cannot be observed. Based on our systematic measurements, the optimal distance is found to the 8 cm, and the experiments were conducted at this monitoring distance.

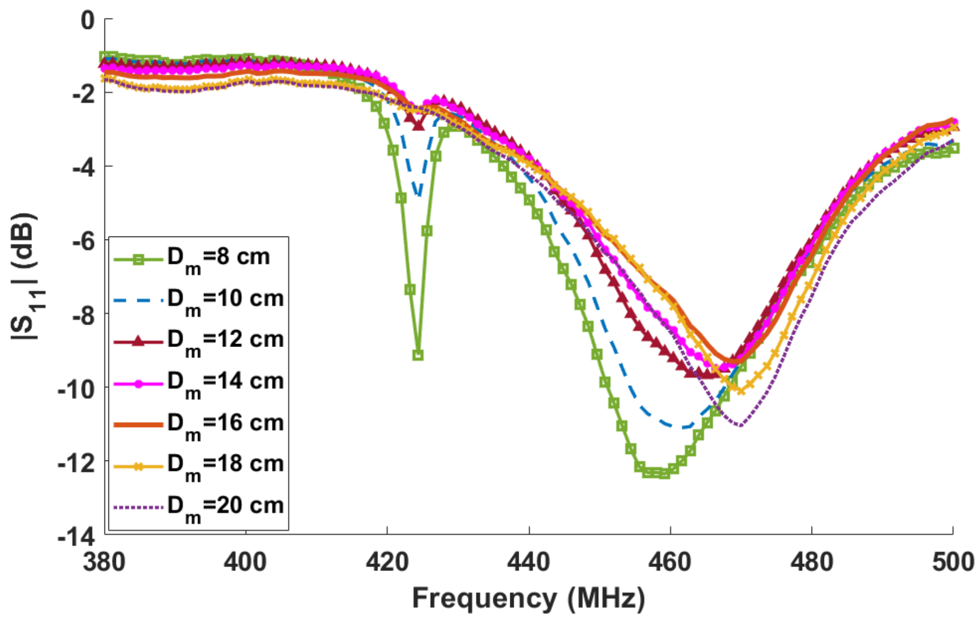

Figure 4.10: Antenna reflection spectrum for varied monitoring distance between the antenna and the sensor (D_m).

Another situation examined is the vibration amplitude ranges that can be followed depending on D_m. To define the vibration amplitude tracking range depending on D_m, the tracking threshold must be determined. Firstly, a reference curve is selected, which is the no vibration state. For this case, the $|S_{11}|_{ref}$ magnitude curve is considered. When a vibration in the form of a peak-to-peak voltage, is applied to the system, the sensor moves up and down around the initial flat plane where it is placed. During this movement, when the voltage reaches the maximum amplitude, the distance between the sensor probes d decreases the most and the frequency of the dip point indicating the presence of the sensor decreases. We call it as $|S_{11}|_{min}$. Conversely, when the voltage goes to the minimum amplitude, the distance d increases, and the frequency of the dip point indicating the presence of the sensor increases. We call it as $|S_{11}|_{max}$. For each D_m value, vibration amplitudes in the range of 1-10 V_{pp} were applied and these three curves were recorded, and the conditions $|S_{11}|_{min}$-$|S_{11}|_{ref}$ and $|S_{11}|_{max}$-$|S_{11}|_{ref}$ were examined. $|S_{11}|_{min}$-$|S_{11}|_{ref}$ curves show a local maximum, while $|S_{11}|_{max}$-$|S_{11}|_{ref}$ curves show a local minimum. The purpose of this calibration is to reduce the effect of clutter. Next, the local peak and dip magnitude values for each case were examined, and the trackable dB value was determined, which is called the tracking threshold. In this study, we selected it as 0.1 dB. Since the clutter effect is minimal, system sensitivity is high and the threshold is quite low. Cases with a magnitude value below this threshold cannot be sensed. The reference, minimum and maximum curves are given in Figure 4.11(a) when D_m is 8 cm. Figure 4.11(b) contains curves for different vibration amplitudes as a result of the operation. The range of sensed vibration amplitudes is plotted for various monitoring distances in Figure 4.12, with a tracking threshold of 0.1 dB. It can be observed from Figure 4.12 that the detectable vibration amplitude decreases as the distance between the antenna and the sensor increases. When D_m is 8 cm, 0.07-0.7 mm range which is corresponding to 1-10 V_{pp} range, is fully sensed, when D_m is 16 cm and above, sensor presence disappears and frequency shifts cannot be detected.

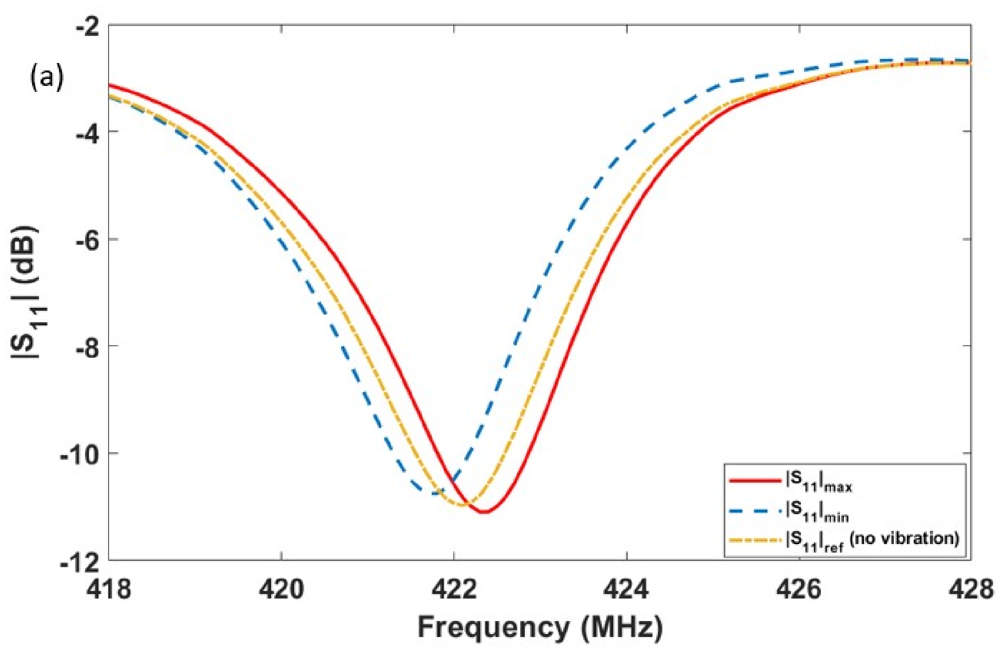

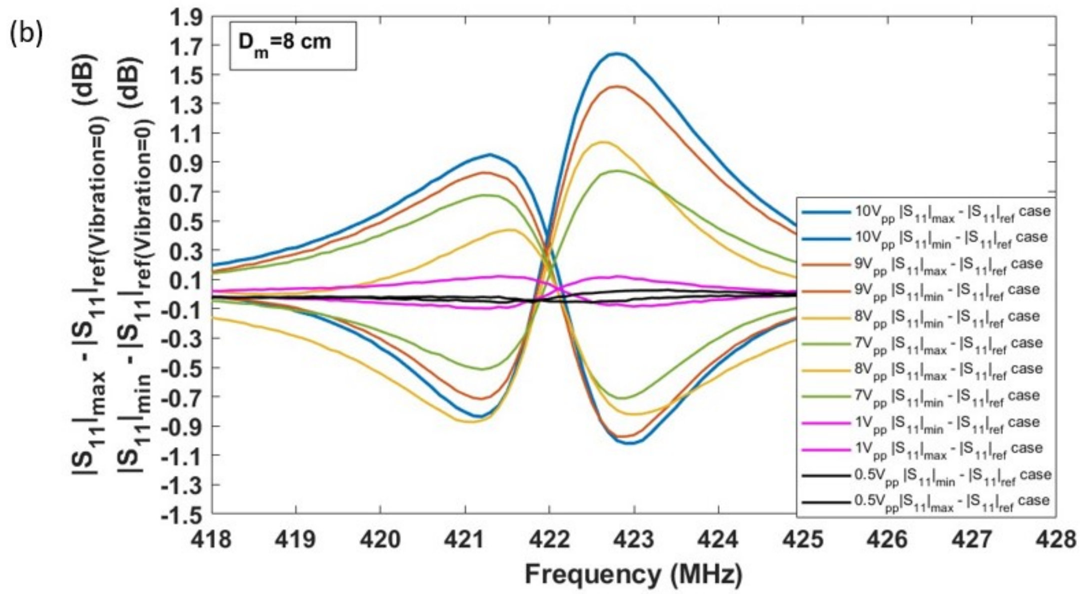

Figure 4.11: (a) $|S_{11}|$ curves obtained from the cases of vibration (maximum and minimum situations) and no vibration (b) $|S_{11}|$ curves subtracted from the reference curve for different vibration amplitudes when D_m=*8* cm.

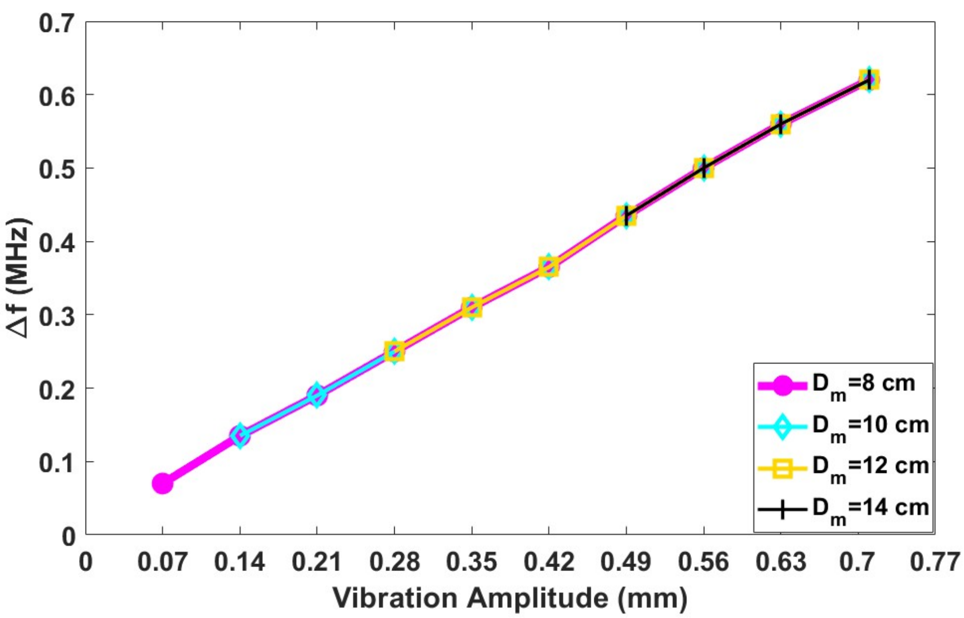

Figure 4.12: Range of vibration amplitudes detected by the wireless detection system for various monitoring distances with a tracking threshold of 0.1 dB.

4.4 Sensitivity

Sensitivity is defined as the ratio of the change in resonance frequency to the corresponding change in amplitude, or equivalently, as the slope of the actual vibration amplitude-frequency curve. Besides, the sensitivity value is equal to the ratio given in (4.1) because this gives the frequency response per the amplitude change with a distance unit. Note that although sensitivity can be expressed in different units, we express vibration in terms of displacement, and it is more logical to use a distance unit. As a result, we define the sensitivity in the units of MHz/mm. Figure 4.13 shows the frequency shifts measured wirelessly vs the actual imaged distance differences. The sensitivity values for each sensor system are given in Table 4.4. Considering the antenna resonance frequency and the position of the sensors according to the frequency values in the antenna operating band (Figure 4.2), the sensitivity values of the systems make sense. The 25-strip sensor resonance frequency is the closest to the antenna operating frequency. Therefore, the sensitivity of this system yields the highest sensitivity, 1.025 MHz/mm. Since 28-strip sensor's resonance frequency is the farthest, the sensitivity value of it is the smallest.

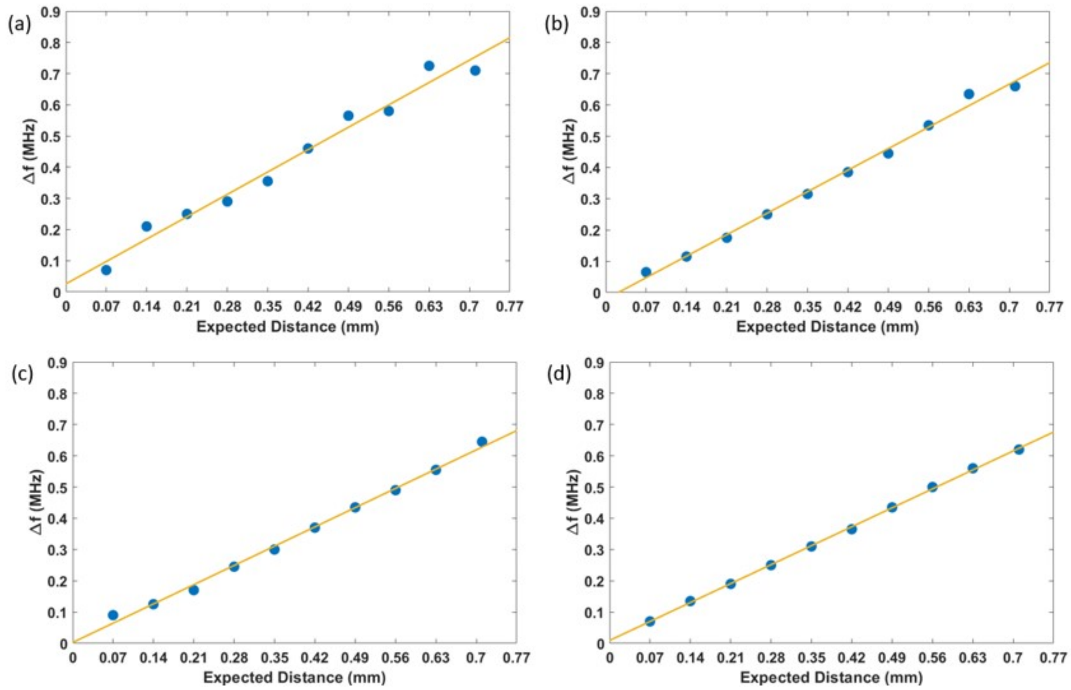

Figure 4.13: Measured frequency shift vs the actual imaged distance difference for (a) 25-, (b) 26-, (c) 27- and (d) 28-strip sensor.

Table 4.4: Sensitivity levels of our wireless systems using different sensors.

	System with 25-strip Sensor	System with 26-strip Sensor	System with 27-strip Sensor	System with 28-strip Sensor
Sensitivity (MHz/mm)	1.025	0.983	0.880	0.866

4.5 Error

We investigated the average deviation of distance data measured with our sensor from the actual distance. We utilized the mean absolute error (MAE) metric to quantify the errors. The MAE is a metric used to evaluate the accuracy of a prediction model. It measures the average size of the errors in a set of predictions, regardless of whether the errors are positive or negative. Specifically, it is calculated as the average of the absolute differences between the predicted values and the actual observations in a test sample, with each difference given equal weight (4.3). Experimental test results, *dist*, are subtracted from the real value for all input values, y_i ,and the absolute value is taken. For each input state, these values are summed and divided by the total number of data, n. Table 4.5 shows the results for the systems obtained with each sensor.

$$MAE = \frac{\sum_{i=1}^{n} |y_i - dist_i|}{n} \tag{4.3}$$

Apart from this error calculation, the data is numerically very small. Therefore, it is more acceptable to compare the expected results with the experimental data as a percentage. At this point, the mean average percentage error (MAPE) is calculated using (4.4). The mean average percentage error (MAPE) is the computed average of percentage errors by which forecasts of a model differ from actual values of the quantity being forecast. The MAPE of less than 5 % indicates that the forecast is considered acceptably accurate. The MAPE greater than 10 % but less than 25 % indicates low but acceptable accuracy.

$$MAPE = \frac{1}{n}(\sum_{i=1}^{n} \left| y_i - \frac{dist_i}{y_i} \right| * 100) \tag{4.4}$$

y_i is the expected value (real value), $dist_i$ is the experimental value and n is the number of data.

Table 4.5: System error values.

	System with 25-strip Sensor	System with 26-strip Sensor	System with 27-strip Sensor	System with 28-strip Sensor
Average Absolute Error (mm)	0.028	0.027	0.009	0.007
Average Percentage Error (%)	10.489	5.025	6.286	1.181

4.6 Resolution

We focus on analyzing the sensor's ability to measure the minimum change in vibration amplitude that is detectable, which is defined as its resolution. The resolution is determined as the smallest vibration amplitude change that can be detected despite noise.

In this experiment, the purpose is to discover the minimum difference between two fully distinguishable amplitude values. For this aim, 8 V_{pp} operating point was taken as the reference point. The minimum amplitude greater than 8 V_{pp} but completely distinguishable from 8 V_{pp} was investigated using error bars. Experiments were performed with enough sample size to be considered statistically correct to find this detectable difference. At each voltage, the experiments were repeated 10 times with appropriate intervals by stopping the system between each measurement so that the experiments would not affect each other. The standard deviation error bars were examined, and the minimal non-overlapping difference that was completely distinguishable from each other was investigated. Figure 4.14 illustrates the findings from the experiments conducted to evaluate the sensing system's resolution. The distance information Δd corresponding to each frequency shift Δf values obtained as a result of the experiment repeated every 10 times at one voltage value was calculated using the formulas 4.1 and

4.2. The actual distance obtained as a result of the imaging vibration amplitude experiment was used as the x-axis. Using this information, mean and standard deviation calculations were performed using MATLAB and error bars were drawn as seen in Figure 4.15. According to the standard deviation error bar of reference vibration amplitude (0.56 mm) which was corresponding to 8 V_{pp}, the closest non-overlapping standard deviation error bar was determined. Thus, it was assumed that statistically existing data can be distinguished from each other. The mean of the Δd forming standard deviation error bar was taken separately for both reference and other vibration amplitude. The difference between these two means was taken as the resolution. In Figure 4.15(a), it can be seen in detail the non-overlapping error bar status, the mean of Δd values corresponding to the applied vibration amplitude in distance unit, and how the resolution is obtained, and this procedure is valid for all sensors. As seen in Table 4.6, our wireless systems using different sensors have resolution values at tens of micrometers, which indicates that vibration amplitude values can be differentiated with several tens of micrometer difference. As seen in Table 4.6, our wireless systems using different sensors have resolution values at tens of micrometers, which indicates that vibration amplitude values can be differentiated with several tens of micrometer difference.

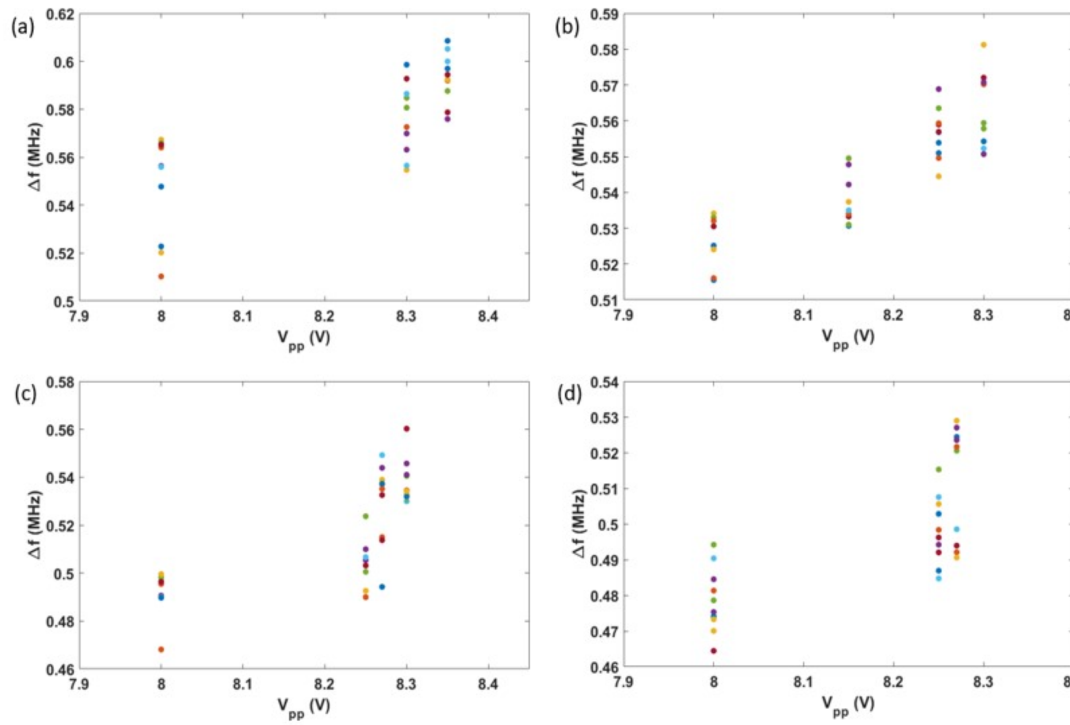

Figure 4.14: Measurements repeated for statistical accuracy using (a) 25-, (b) 26-, (c) 27- and (d) 28-strip sensor.

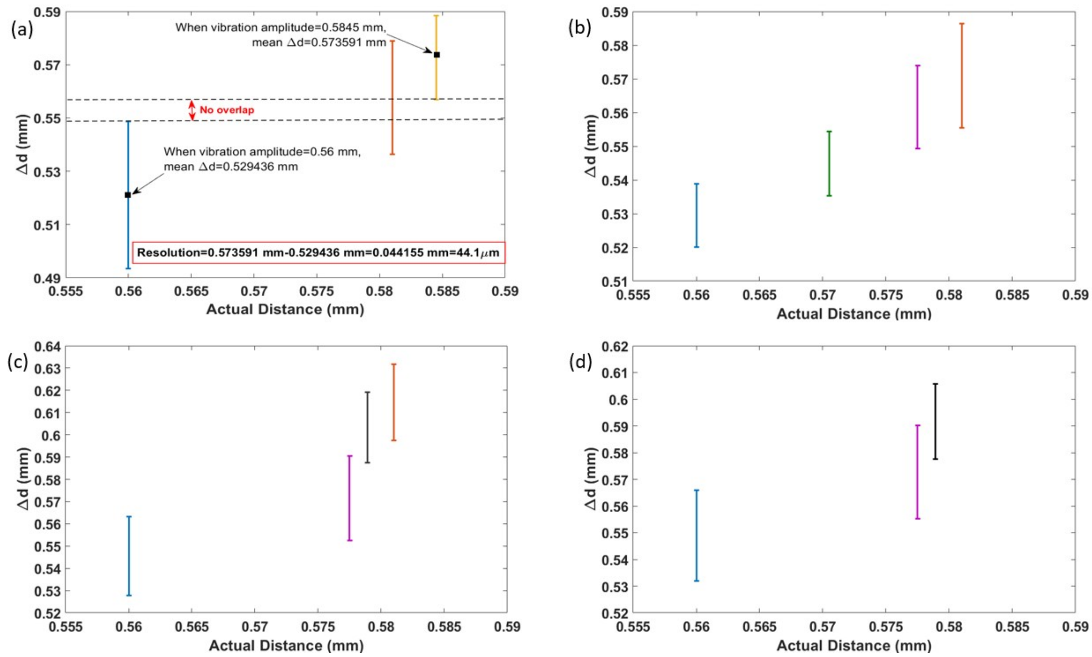

Figure 4.15: Standard deviation error bars obtained using (a) 25-, (b) 26-, (c) 27- and (d) 28-strip sensor.

Table 4.6: Resolution for our wireless systems.

	System with 25-strip Sensor	System with 26-strip Sensor	System with 27-strip Sensor	System with 28-strip Sensor
Resolution (μm)	44.1	30.0	42.2	38.4

Chapter 5

Wireless Multi-Sensor Vibration Detection by a Single Transceiver Antenna

The fundamental concept of multipoint sensing using a single antenna is to establish simultaneous connections between the antenna and sensors in the array. For a single sensor, the antenna transmits electromagnetic waves to the sensor and receives the scattered waves. For an array of sensors, the antenna illuminates each sensor in the array and gathers the waves that are scattered back. Each sensor that has a unique resonance frequency in the array is defined around its resonance frequency. While the sensor structures used are the same, sensors with different resonance frequencies are obtained by changing the number of strips at each sensor. With no spectrum overlap, this configuration establishes an electromagnetic channel between the antenna and each sensor in the array. As a result, it can be achieved to create a multipoint sensing system using a single antenna that can simultaneously receive data from all of the sensors.

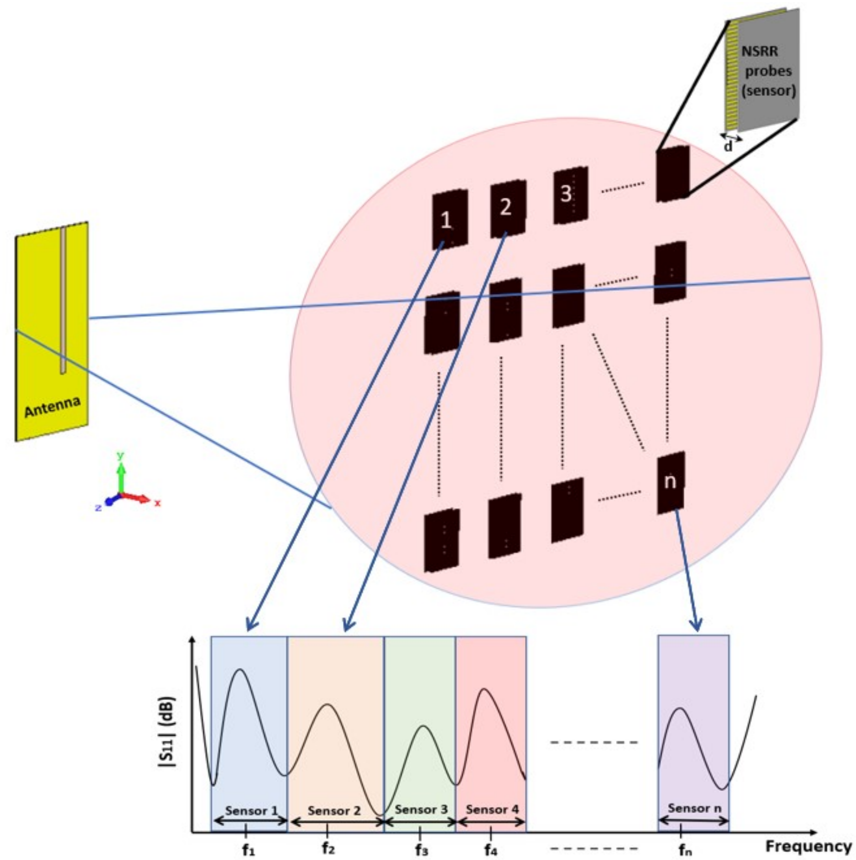

Figure 5.1: Proposed multipoint wireless sensing system using n sensors, each having a pair of NSRR probes with a unique resonance frequency. The antenna reflected spectrum shows how each sensor uniquely responds to a dedicated spectral region for local wireless sensing.

The fundamental idea of the detection system is shown in Figure 5.1. As seen in this figure, a single antenna illuminates the sensor array directly. Due to the coupling of the array elements and the antenna, the behaviour of each sensor can be monitored in the reflectance spectrum of the antenna, as in the case of the system using a single antenna and a single sensor. Each sensor appears as a local peak or dip around its specific frequency in the antenna reflection coefficient spectrum. Thanks to these specific frequency values, the sensors are detected individually.

5.1 Inter-coupling between the Multiple Vibration Sensors

An essential factor in array configurations is the inter-coupling among the multiple sensors, which modifies the capacitance between the antenna and the sensors in the system. Therefore, the capacitance of the system is affected, which causes deviations in frequency shifts and adversely affects the characteristic behavior of the system. As the sensors are closer together, this inter-coupling increases and deteriorates the system's operating performance. The significant point is to find the minimum distance so that there is no inter-coupling among the sensors and hence, each only sensor interacts with the antenna.

Several methods have been followed in the experiments to make the system work without inter-coupling. First, 4 sensors were placed opposite corners of the antenna. Sensors with close resonance frequencies were positioned diagonally away from each other so that the distance between them is maximum. Since the sensors were far from the junction of the antenna feed line and the antenna slot, the system's quality factor decreased. It became difficult to detect the sensors in the antenna reflection spectrum. Then, as a continuation of the first experiment, the sensors were moved to the right, left, up, and down. The inter-coupling was observed as diminishing as the distance between the two NSRR probes was increased. Also, the performance improved as the antenna was now closer to the region that we desired to illuminate. It has been observed that the distance between the sensors must be 4 cm or more at the frequency band we are working. Moreover, as mentioned before, the strips on the probes are parallel in the z direction, so that the strips are parallel with the electric field direction and the highest coupling is achieved. The sensors that are located side by side in the z direction are not perfectly aligned in the same line, that is, they are moved in the y direction. Thus, the inter-coupling between the sensors was reduced in this way as well. Finally, after many systematic trials the sensor were placed as seen in Figure 5.2. In this placement, the distances between the sensors were adjusted to be 4 cm and longer. As given in Figure 5.3, when the distance between the sensors is 4 cm or longer and the antenna is brought closer to region that we aim to illuminate, each sensor can be more easily detected in the antenna reflection spectrum.

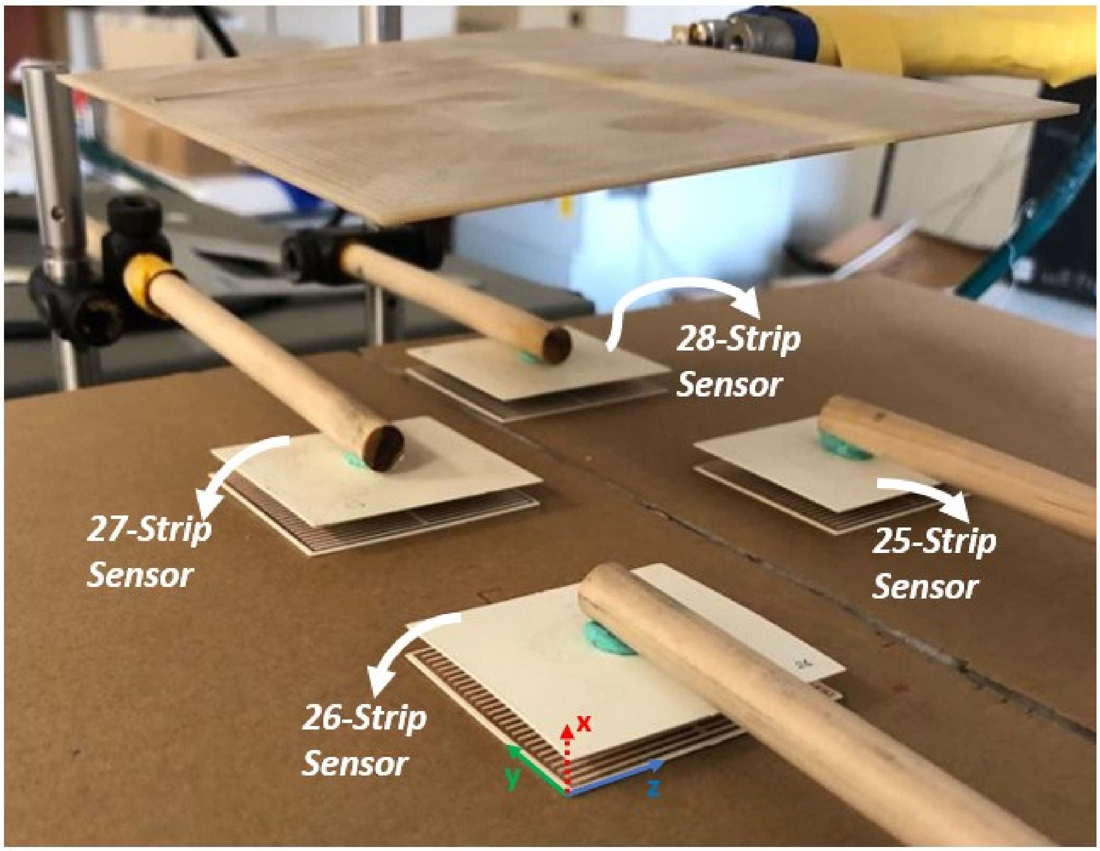

Figure 5.2: Inter-coupling experiment setup using 4 sensors. The distance between the 25- and the 26-strip sensors is 5.0 cm, the distance between the 26- and the 27-strip sensors is 4.0 cm, the distance between 27- and 28-strip sensors is 4 cm, and the distance between 25- and 28-strip sensors is 4.5 cm (All distances are measured corner to corner.)

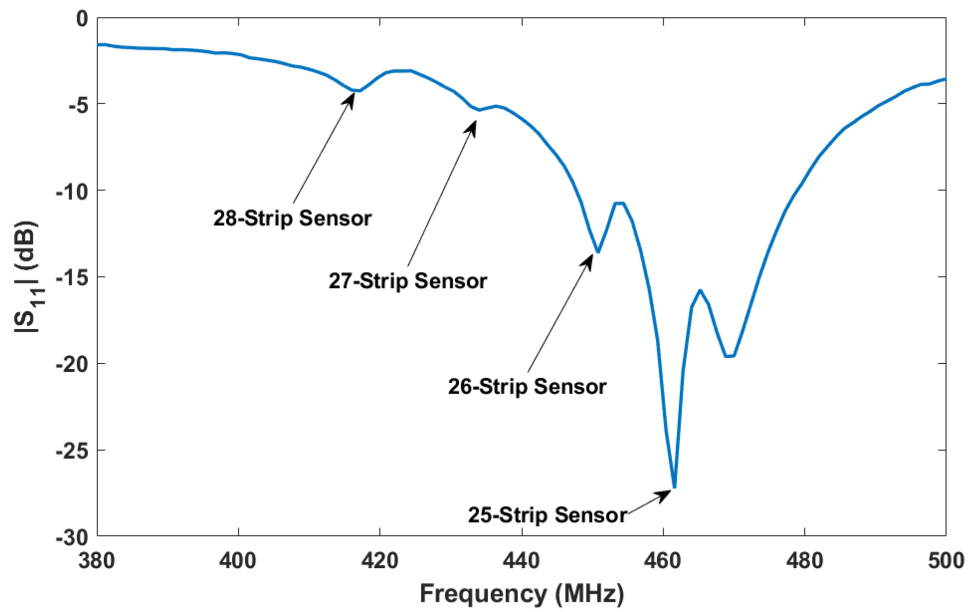

Figure 5.3: Antenna reflection spectrum of the array structure built with 4 sensors.

5.2 Vibration Detection with Array System

Experiments were performed using multiple sensors using a single antenna and detecting vibration from each sensor separately using final configuration shown in Figure 5.2. A loudspeaker was used again to generate vibration. When it was desired to apply different amplitudes of vibrations, an experimental setup was established with two speakers and a signal generator or two signal generators. Different strip numbers of sensors were used to separate the spectral detection regions uniquely corresponding to each sensor, as explained in the previous section. Figure 5.3 exhibits four distinct local dips corresponding to each sensor in the reflection wave spectrum of the antenna. Although the dips corresponding to each of the four sensors are apparent, the strength of the coupling differs for each resonance, relation between the antenna bandwidth and the resonance frequency of each sensor.

Sensors are less illuminated at the edge frequency values of the antenna bandwidth, which reduces coupling. On the other hand, when the antenna sees NSRR probes, it is also possible to monitor spectrally the features on the reflection spectrum, which makes wireless detection possible. The concept of multipoint sensing with a single antenna relies on assigning specific resonance frequencies (f_{res}) and frequency shifts (Δf) for each sensor in advance. The number of sensors in the array depends on the antenna bandwidth and Δf. In this way, $n = BW/\Delta f$ determines ideally how many sensors can be sensed with the antenna used [39]. Four sensors were used in our experiments. Various experiments were carried out when D_m was 8 cm. First, a vibration signal with the same amplitude and frequency was applied to all sensors. As a result of this application, frequency shifts were observed in all sensor ranges in the antenna reflection spectrum, as seen in Figure 5.4. Data were acquired over the entire range. The Δf range for each sensor was examined separately.

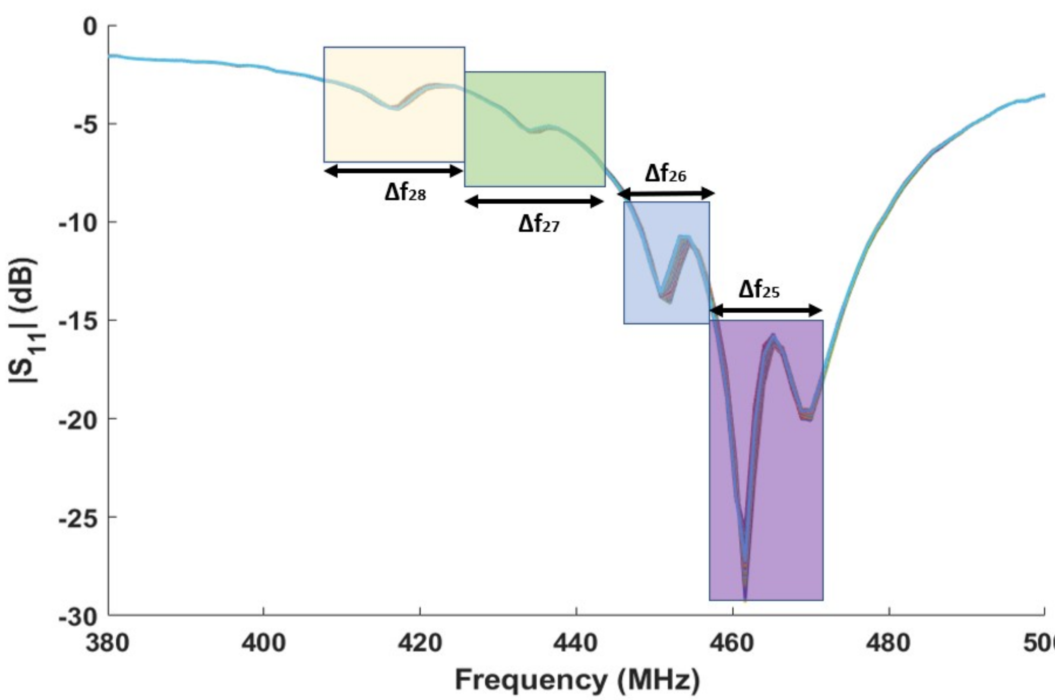

Figure 5.4: Frequency shifts for each sensor in the sensor array when applying a 5 Hz and 10 V_{pp} sinusoidal vibration signal.

For each sensor, vibrations from 1 to 10 V_{pp} at a frequency of 5 Hz were applied and frequency shifts were measured for each case separately. Calculations were made for each sensor forming the array using the calculation method presented in Chapter 4. As a result of these calculations using the measured spectrum, we found that, the sensors used in the array exhibit the same characteristics as when they are used individually, which indicates that the sensors in the array can be distinguished individually and give accurate results for vibration sensing even when used together. Table 5.1 shows the figure-of-merits of the sensors that make up the array. Each sensor in the array delivered performance in agreement with their previous individual cases.

Table 5.1: Figure-of-merit comparison of each sensor under the same vibration exposure.

	25-Strip Sensor	26-Strip Sensor	27-Strip Sensor	28-Strip Sensor
Average Absolute Error (mm)	0.016	0.009	0.062	0.014
Sensitivity (MHz/mm)	0.926	1.287	0.733	1.082
R^2	0.989	0.997	0.993	0.991
Average Percentage Error (%)	6.231	3.401	6.594	4.943

In the second group of experiments, two speakers and one signal generator were used. 25- and 28-strip sensors were placed on the same vibration source; on the other side, 26- and 27-strip sensors were placed on the other vibration source. The speaker with 25- and 28-strip sensors was fed with 5 Hz and 10 V_{pp} vibration. The other speaker was held still, there was no movement. As seen in Figure 5.5, while there were shifts around the frequency of 25- and 28-strip sensors, no frequency shift occurred in the other sensors. When the distance calculations were made as mentioned above, results close to the expected results were obtained.

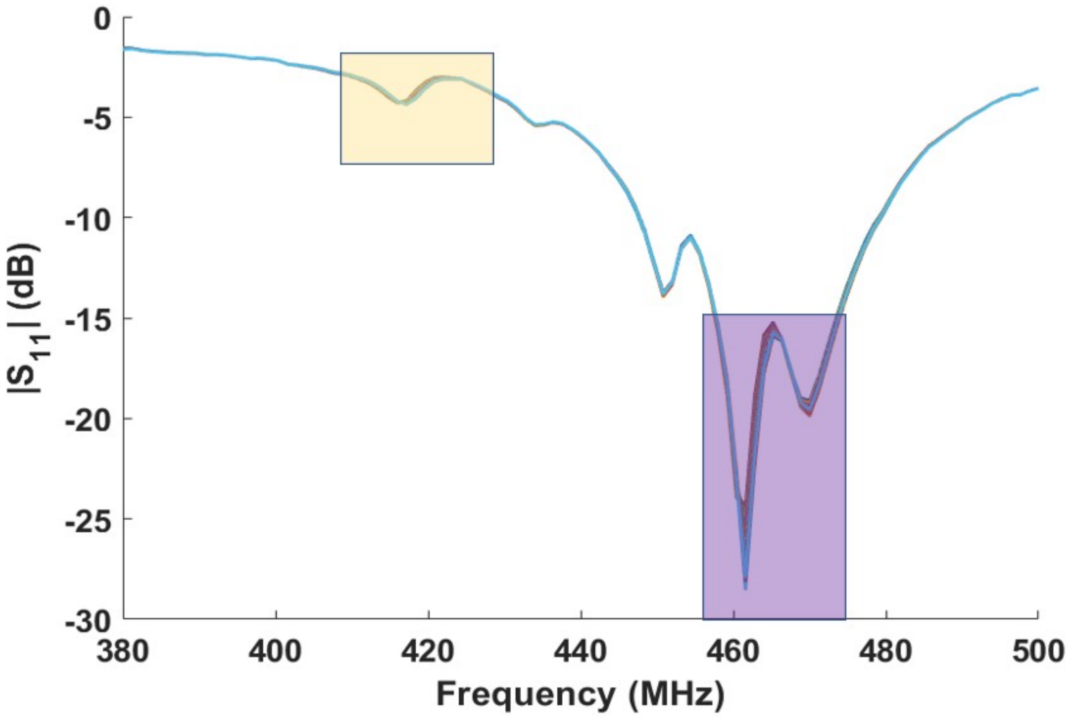

Figure 5.5: 25- and 28-strip sensors vibrate while the other sensors remain stationary.

The same experiment was performed by applying vibration to 26- and 27-strip sensors at 5 Hz and 10 V_{pp} while keeping the other sensors stationary. The expected results were obtained in terms of distance with low error percentages, 26-strip sensor working with an average percentage error of 2.55 %, while 27-strip sensor gave results with an error of 4.33 %. In other experiments, different vibrations were applied to the sensors. For example, 5 Hz and 10 V_{pp} sinusoidal vibrations are applied to 25- and 28-strip sensors, while 11 Hz and 10 V_{pp} sinusoidal signals were applied to 26- and 27-strip sensors. During this application, the velocity due to the frequency difference was observed. The movement took place faster in the application at a higher frequency value. Apart from that, 5 Hz and 10 V_{pp} sinusoidal signals were applied to 25- and 28-strip sensors, while 5 Hz and 5 V_{pp} sinusoidal signals were applied to 26- and 27-strip sensors. During this application, the change in frequency shift due to amplitude difference was observed and distance information was examined. Apart from these experiments, different types of signals can be applied. Some sensors can be given a sinusoidal signal, while others can be given a rectangular waveform, and these different signals can be observed in time domain and FT analyses. When the time domain was examined, the superposition cross-term of the applied signals were seen. When the FTs were examined, the maximum amplitude was observed at the applied frequency values, while peaks were observed in the harmonics depending on the signal type. As a result of these experiments, vibration detection was performed with a single antenna using sensors at different resonance frequencies. Different types of signals and frequency shifts in different spectral regions in response to different amplitudes of local vibration when each sensor was placed were detected through using all of the sensors. This shows that the sensors could be used to sense vibration by many sensors in the form of an array index the appropriate inter-coupling condition. Thus, data can be received in larger areas with many probes but using only one transceiver antenna or the antennas can also be repeated each to cover a dedicated array of multiple sensor. Such a giant wireless system of multi-antennas and multi-sensor arrays hold great promise to wirelessly detect vibration propagation over large surfaces.

Chapter 6

Conclusion and Future Work

This thesis proposes a wireless sensing system for detecting vibrations. In this system, the sensor architecture consists of a pair of nested ring resonator probes. The electromagnetic coupling between these probes and transceiver antenna results in enhanced sensitivity and resolution compared to similar sensors reported in the literature. Furthermore, the proposed system is straightforward to produce and cost-effective. The design of this system is based on near-field coupling of the NSRR probes figure-of-merits to improve key including sensitivity, resolution, and linearity. These wireless sensors exhibit high linearity. The detection system can monitor vibration signals of different types and with different characteristics. The proposed vibration sensor technology offers a high resolution to detect vibration amplitudes ranging at µm scale. For the sensing system, it has been determined that the maximum amplitude of vibrations can be detected in the vertical direction with respect to the NSRR probe according to the experiment's results to determine the distance d between the two plates of the sensor in the mm range.

In this operation, one of the NSRR probes is adhered to the surface of the vibration source, and the other part is fixed opposite. When vibration occurs, the capacitance change depending on the distance change between the two probes appears as a frequency shift in the antenna reflection spectrum. Different types of vibration signals can be applied and observed through the sensor. The wireless detection system, which senses the displacement caused by the vibration amplitude, is fed with signals of different amplitudes. The vibration amplitude change causes a linear change in the frequency shift. The coefficient of determination, R^2 is 0.99 or better. 25-strip sensors exhibit a sensitivity level of 1.025 MHz/mm, which is the best performance level among all studied sensors. The percentage error values for all systems vary between 1.18-10.49 %. When the 4 systems used are compared, the best resolution of 30 µm is obtained from the system constructed with 26-strip sensors. The maximum vibration amplitude varies depending on both the experimental setup and the distance between the sensor parts. For this whole sensing system, the monitoring distance, D_m, between the sensor and the antenna plays an important role. As D_m increases, the sensor disappears in the reflection spectrum. Experiments were carried out by choosing the optimal distance of 8 cm. Preferring different antennas or sensor geometries can increase D_m, but this increase may not be very significant. These findings show that the proposed wireless low-cost vibration sensors are promising for industrial applications.

Another wireless sensing approach that has been proposed in this thesis is to use multiple sensors read out by a single antenna. In this approach, each sensor is assigned a specific resonant frequency and a unique spectral range is reserved for the frequency shift local to where that sensor is placed. This ensures that there is no overlap in the frequency ranges and helps to avoid interference between sensors. Through experimentation, data from multiple sensors was gathered using one antenna, while each sensor maintained its unique characteristics within the array configuration. Here, the detection of vibrations is enabled by the collective output of multiple sensors, and it is straightforward to associate the collected data with each respective sensor.

As a future work, the sensor structure can be developed to detect incoming vibrations in all 3 axes. Currently, the sensor we have can sense the vibration coming on a single plane (perpendicular to the sensor). Theoretically, the sensor can sense the vibration parallel to. At third-axis detection can be achieved by changing the sensor positioning or by changing the sensor architecture. Apart from this, the distance between two plates can be increased up to cm level in the designed sensor. This distance can be increased for the sensor by changing both the thickness and the dielectric coefficient using different types of substrate. Another step that can be considered in the future may aim to increase the monitoring distance. The maximum D_m achieved using the sensors designed in the experiments was 16 cm, which can be considered relatively short distance for some real applications. One possible approach to increasing the D_m could be based on the deployment of semi-passive devices. Such devices are commonly used in RFID and energy harvesting applications. One approach is to incorporate energy harvesting, whereby the NSRR probe structure serves as a semi-passive structure that converts the RF signal into DC bias current and utilizes an internal transmitter to reflect the signal. Moreover, for the array structure, this innovative multi-point single antenna detection scheme boasts high sensitivity and resolution, making it a promising candidate for future applications such as two-dimensional surface vibration mapping of industrial materials, which can enable the detection of damage or deformation over the surface or other places.

Appendix A

Coefficient of Determination (R^2)

The coefficient of determination, or R^2, is a metric that can be used to quantify the linearity of a curve. R^2 is a statistical measure that depicts how far an actual curve deviates from a fitted linear curve. To compute R^2, a linear curve is fitted to a set of observed data points, where each data point is labelled as y_i, the corresponding fitted value as $\widehat{y_I}$, and the mean of the observed data as $\widehat{y}$. R^2 can be defined as

$$R^2=\frac{SRR}{SST} \text{ where } SSR=\sum_i(\widehat{y_I}-\widehat{y})^2 \text{ and } SST=\sum_i(y_i-\widehat{y})^2.$$

Bibliography

[1] Li Zhen, Wu Shujuan, Zhang Guojun, Xue Chenyang, “Finite Element Analysis for a New Kind of MEMS Three-Dimensional Vibration Sensor”, Chinese Journal of Sensors and Actuators, vol. 26, issue 4, 2013, pp. 786-789.

[2] Wang Qingmin, Yang Yaoen, Su Mubiao, Liu Yuhong, “Study on Sensing Characteristics of Micro Capacitive Sensor Based on MEMS”, Chinese Journal of Sensors and Actuators, vol. 22, issue 10, pp. 88-91, 2009.

[3] Aiyin Guo, “A Vibration Sensor Design Research”, Sensors & Transducers, vol. 169, issue 4, pp. 228-234, 2014.

[4] Zhang Xiao-yan, “The Adjustment of Vibration Sensors and the Analysis of Error Margin”, Journal of Shandong Institute of Commerce and Technology, 7(6): 102-106, 2007.

[5] Y. Cao, X. L. Rong, S. J. Shao and K. P. He, ”Present Situation and Prospects of Vibration Sensors,” 2012 International Conference on Computer Distributed Control and Intelligent Environmental Monitoring, Zhangjiajie, China, pp. 515-518,2012.

[6] Chen Jie, Huang Hong, “Sensors and Detective Technology “, Beijing: Higher Education Press, 2002.

[7] Huang Shu-tong, “Study of the Groove Effect of the Sensor for High-Speed Maglev Train”, Southwest Jiao tong University Master Degree Thesis, 2008.

[8] Xu Fu-cheng, “Common Vibration Sensor and its Typical Application Circuit”, Practical Electronics, (10):13-15,2008.

[9] Li Ming-guo, Sun Rong-xiang, Li Yong, “Research on Vibration Sensor of Ultra Low Frequency”, Colliery Mechanical & Electrical Technology, (3):37-39,2008.

[10] Zhang BaiLi, “The Advancement and Application of the Electric Capacity Sensor”, Journal of Xinzhou Teachers University, 21(2):24-26,2005.

[11] Wang Zhao-hua, “Capacitive Sensor based on Active Bridge Circuit and Its Measurement System”, Beijing University of Chemical Technology Master Degree Thesis, 2006.

[12] J. S. Roundy, “Energy scavenging for wireless sensor nodes with a focus on vibration to electricity conversion”, Dissertation, University of California at Berkeley, 2003.

[13] J. O. Miranda, “Electrostatic vibration-to-electric energy conversion”, Dissertation, Massachusetts Institut of Technology at Boston, 2004.

[14] Sun Sheng-he, “Development trend of modern sensor”, Journal of Electronic Measurement and Instrument, 23(1):1-10,2009.

[15] Zhang Yan, Zeng Guang-yu, “Application and Development of the Photoelectric Sensor”, Sci-Tech Information Development & Economy, 16(13):254-255, 2006.

[16] Shuqing Han , Jianhua Zhang, Mengshuai Zhu, Jianzhai Wu, Chen Shen ,Fantao Kong, “ Analysis of the frontier technology of agricultural IoT and its predication research”, IOP Conference Series Materials Science and Engineering, 231(1):012072.

[17] Mehmet Yılmaz, Oğuz Tekelioğlu, Saadettin Yıldırım, Mustafa Çetin, “Physical Principles of Vibration and Measurement Techniques”, GOÜ. Ziraat Fakültesi Dergisi,21 (2), 71-79, 2004.

[18] Tao Chen, Suyan Li, Hui Sun, “Metamaterials application in sensing”, Sensors 2012, 12, 2742–2765.

[19] R. Melik, E. Unal, N. K. Perkgoz, C. Puttlitz, and H. V. Demir, “Metamaterial based telemetric strain sensing in different materials”, Opt. Exp. 18, 5000- 5007, 2010.

[20] R. Melik, E. Unal, N. K. Perkgoz, C. Puttlitz, and H. V. Demir, “Flexible metamaterials for wireless strain sensing”, Appl. Phys. Letters 95, p. 181105, 2009.

[21] Burak Ozbey, Emre Unal, Hatice Ertugrul, Ozgur Kurc, Christian M. Puttlitz , Vakur B. Erturk, Ayhan Altintas and Hilmi Volkan Demir, “Wireless Displacement Sensing Enabled by Metamaterial Probes for Remote Structural Health Monitoring”, Sensors 2014, 14(1), 1691-1704.

[22] Kairm, H., Delfn, D., Shuvo, M. A. I., Chavez, L. A., Garcia, C. R., Barton, J. H., “Concept and model of a metamaterial-based passive wireless temperature sensor for harsh environment applications”, IEEE Sensors Journal, 15(3), 1445–1452.

[23] Chen, HT., Padilla, W., Cich, M. et al.,”A metamaterial solid-state terahertz phase modulator” , Nature Photon 3, 148–151, 2009.

[24] Basudev Lahiri, Ali Z. Khokhar, Richard M. De La Rue, Scott G. McMeekin, and Nigel P. Johnson, “Asymmetric split ring resonators for optical sensing of organic materials,” Opt. Express 17, 1107-1115, 2009.

[25] S. Jagan Mohan Rao, Rakesh Sarkar, Gagan Kumar, and Dibakar Roy Chowdhury, “Gradual cross polarization conversion of transmitted waves in near field coupled planar terahertz metamaterials,” OSA Continuum 2, 603-614, 2019.

[26] Yang, Y., Huang, R., Cong, L., Zhu, Z., Gu, J., Tian, Z., et al. (2011), “Modulating the fundamental inductive-capacitive resonance in asymmetric double-split ring terahertz metamaterials”, Applied Physics Letters, 98(12), 121,114.

[27] C. R. Farrar and K. Worden, ”An introduction to structural health monitoring”, Philos. Trans. Roy. Soc. London A Math. Phys. Sci., vol. 365, no. 1851, pp. 303-315, 2007.

[28] A. Sabato, C. Niezrecki and G. Fortino, "Wireless MEMS-Based Accelerometer Sensor Boards for Structural Vibration Monitoring: A Review," in IEEE Sensors Journal, vol. 17, no. 2, pp. 226-235, 15 Jan.15, 2017.

[29] J. B. Pendry, A. J. Holden, D. J. Robbins, and W. J. Stewart, "Magnetism from conductors and enhanced nonlinear phenomena," IEEE Transactions on Microwave Theory and Techniques, vol. 47, no. 11, p. 2075, 1999.

[30] H.-J. Lee and J.-G. Yook, "Biosensing using split-ring resonators at microwave regime," Appl. Phys. Lett., vol. 92, p. 254103, 2008.

[31] R. Melik, E. Unal, N. K. Perkgoz, B. Santoni, D. Kamstock, C. Puttlitz, and H. V. Demir, "Nested metamaterials for wireless strain sensing," IEEE J. Sel. Topics Quantum Electron., vol. 16, pp. 450–458, 2010.

[32] Sikha Simon K., Sreedevi P. Chakyar, Jolly Andrews, and Joseph V. P., "Metamaterial split ring resonator as a sensitive mechanical vibration sensor", AIP Conference Proceedings 1849, 020021, 2017.

[33] Sikha K. Simon, Sreedevi P. Chakyar,Anju Sebastian1, Jovia Jose, Jolly Andrews, V. P. Joseph, "Broadside Coupled Split Ring Resonator as a Sensitive Tunable Sensor for Efcient Detection of Mechanical Vibrations", Sensing and Imaging, 0:17, 2019.

[34] Ekmekci E., & Turhan-Sayan G., "Multi-functional metamaterial sensor based on a broad-side coupled srr topology with a multi-layer substrate", Applied Physics A, 110(1), 189–197,2013.

[35] Marqués, R., Mesa, F., Martel, J., & Medina, F., "Comparative analysis of edge-and broad-side-coupled split ring resonators for metamaterial design-theory and experiments", IEEE Trans-actions on Antennas and Propagation, 51(10), 2572–2581, 2003.

[36] A. Vivek, K. Shambavi and Zachariah C. Alex, "A review: metamaterial sensors for material characterization", in Sensor Review, December 2018.

[37] F. Falcone, T. Lopetegi, J. D. Baena, R. Marqu´es, F. Mart´ın, and M. Sorolla, "Effective negative-/spl epsiv/stopband microstrip lines based on

complementary split ring resonators," IEEE Microwave and Wireless Components Letters, vol. 14, no. 6, p. 280, 2004.

[38] T. Koschny, M. Kafesaki, E. Economou, and C. Soukoulis, "Effective medium theory of left-handed materials," Physical review letters, vol. 93, no. 10, p. 107402, 2004.

[39] B. Ozbey, V. B. Ertürk, O. Kurc, A. Altintas and H. V. Demir, "Multi-Point Single-Antenna Sensing Enabled by Wireless Nested Split-Ring Resonator Sensors," in IEEE Sensors Journal, vol. 16, no. 21, pp. 7744-7752, Nov.1, 2016.

[40] B. Ozbey, H. V. Demir, O. Kurc, V. B. Erturk, A. Altintas, "Wireless Measurement of Elastic and Plastic Deformation by a Metamaterial-Based Sensor", Sensors, vol. 14, pp 19609-19621, 2014.

[41] S. I. Latif, L. Shafai, and S. K. Sharma, "Bandwidth enhancement and size reduction of microstrip slot antennas," IEEE Transactions on Antennas and Propagation, vol. 53, no. 3, p. 994, 2005.

[42] B. Ozbey, A. Altintas, H. V. Demir and V. B. Ertürk, "An Equivalent Circuit Model for Nested Split-Ring Resonators," in IEEE Transactions on Microwave Theory and Techniques, vol. 65, no. 10, pp. 3733-3743, Oct. 2017.

[43] R. A. Dalke, C. L. Holloway, P. McKenna, M. Johansson, and A. S. Ali, "Effects of reinforced concrete structures on RF communications," IEEE Trans. Electromagn. Compat., vol. 42, pp. 486–496, Nov. 2000.